JCB Journal of Cell Biology

ARTICLE

XAF1 promotes colorectal cancer metastasis via VCP–RNF114–JUP axis

Ji Xia[1], Ning Ma[2], Qian Shi[3], Qin-Cheng Liu[4], Wei Zhang[4], Hui-Jun Cao[1], Yi-Kang Wang[1], Qian-Wen Zheng[1,5], Qian-Zhi Ni[1], Sheng Xu[1], Bing Zhu[1], Xiao-Song Qiu[1,5], Kai Ding[1], Jing-Yi Huang[1], Xin Liang[1], Yu Chen[1], Yan-Jun Xiang[6], Xi-Ran Zhang[1], Lin Qiu[1], Wei Chen[7], Dong Xie[1,5,8], Xiang Wang[9], Lingyun Long[1], and Jing-Jing Li[1,8]

Metastasis is the main cause of colorectal cancer (CRC)-related death, and the 5-year relative survival rate for CRC patients with distant metastasis is only 14%. X-linked inhibitor of apoptosis (XIAP)-associated factor 1 (XAF1) is a zinc-rich protein belonging to the interferon (IFN)-induced gene family. Here, we report a metastasis-promoting role of XAF1 in CRC by acting as a novel adaptor of valosin-containing protein (VCP). XAF1 facilitates VCP-mediated deubiquitination of the E3 ligase RING finger protein 114 (RNF114), which promotes K48-linked ubiquitination and subsequent degradation of junction plakoglobin (JUP). The XAF1–VCP–RNF114–JUP axis is critical for the migration and metastasis of CRC cells. Moreover, we observe correlations between the protein levels of XAF1, RNF114, and JUP in clinical samples. Collectively, our findings reveal an oncogenic function of XAF1 in mCRC and suggest that the XAF1–VCP–RNF114–JUP axis is a potential therapeutic target for CRC treatment.

Introduction

As reported by Global Cancer Statistics 2020, colorectal cancer (CRC) ranks third in terms of incidence and second in terms of mortality worldwide (Sung et al., 2021). Nearly 900,000 people succumb to CRC annually in the world, and metastatic CRC (mCRC) is a major cause of their death (Sung et al., 2021). Despite current advancements in diagnosis and treatment, the therapeutic outcomes of patients with CRC, especially mCRC, are still poor (Malki et al., 2020). The 5-year relative survival rate for CRC patients diagnosed with localized diseases is 91%, whereas for patients with distant metastasis, only 14% of them could survive >5 years (Siegel et al., 2023). Currently, anti-epidermal growth factor receptor therapy, including the monoclonal antibodies cetuximab and panitumumab, is the main targeted treatment that can be combined with standard chemotherapy for mCRC. For the 50% of mCRC patients with *KRAS/NRAS/BRAF* wild-type tumors, cetuximab and panitumumab, in combination with chemotherapy, can extend median survival by 2–4 mo compared with chemotherapy alone (Biller and Schrag, 2021). However, for ∼40% of patients with *KRAS* sequence variations, effective targeted therapies are not yet available (Zhu et al., 2021). Therefore, these studies highlight the need for the development of efficient therapeutic strategies for *KRAS* mutant mCRC patients.

XAF1, a 33 kD zinc-rich proapoptotic protein (Lee et al., 2014), was originally found to antagonize the anti-caspase activity of XIAP by inducing the nuclear translocalization of cytoplasmic XIAP (Holcik and Korneluk, 2001). Later studies disclose that XAF1 also exhibits multiple functions independent of XIAP, including a XIAP-independent proapoptotic function (Chung et al., 2007). XAF1 is reported to be involved in tumorigenesis (Jeong et al., 2018), tumor progression (Choo et al., 2016), and drug resistance (Wang et al., 2012). However, the role of XAF1 in cancer metastasis remains largely undefined.

VCP (also called p97, Cdc48, CDC-48, or Ter94), a type II AAA family member (ATPase with multiple cellular activities), regulates many cellular processes by promoting protein degradation or deubiquitination via its ATPase activity (Hill et al., 2021; van den Boom and Meyer, 2018). VCP promotes lung cancer

[1]CAS Key Laboratory of Nutrition, Metabolism and Food Safety, Shanghai Institute of Nutrition and Health, University of Chinese Academy of Sciences, Chinese Academy of Sciences, Shanghai, China; [2]Department of Thoracic Surgery, Shanghai Chest Hospital, Shanghai Jiao Tong University School of Medicine, Shanghai, China; [3]Central Laboratory, The First Affiliated Hospital of Huzhou University, Huzhou, China; [4]Department of General Surgery, Fengxian Hospital Affiliated to Southern Medical University, Shanghai, China; [5]School of Life Science and Technology, ShanghaiTech University, Shanghai, China; [6]Department of Hepatic Surgery VI, Eastern Hepatobiliary Surgery Hospital, Naval Medical University, Shanghai, China; [7]Institute of Clinical Medicine Research, Zhejiang Provincial People's Hospital, Hangzhou Medical College, Hangzhou, China; [8]NHC Key Laboratory of Food Safety Risk Assessment, China National Center for Food Safety Risk Assessment, Beijing, China; [9]Key Laboratory of Integrated Oncology and Intelligent Medicine of Zhejiang Province. Affiliated Hangzhou First People's Hospital, Zhejiang University School of Medicine, Hangzhou, China.

Correspondence to Jing-Jing Li: tide7@163.com; Lingyun Long: lylong@sinh.ac.cn; Xiang Wang: wangxiang2021@zju.edu.cn.

metastasis through accelerating IκBα degradation and NF-κB activation (Wang et al., 2021). In addition, VCP promotes hepatocellular carcinoma progression by stabilizing HMGB1, leading to downstream activation of the PI3K/AKT/mTOR signaling pathway (Pu et al., 2022). VCP also exerts a metastasis-promoting function in CRC (Fu et al., 2016), but the underlying mechanism remains largely elusive.

The E3 ubiquitin ligase RNF114, also known as ZNF313, participates in multiple cellular processes, such as embryonic development (Zhou et al., 2021), inflammation (Han et al., 2022), and tumor progression (Han et al., 2013). RNF114 regulates tumor metastasis in cervical (Zhao et al., 2021) and gastric (Feng et al., 2022) cancers. Additionally, RNF114 is identified as a cell-cycle activator in CRC via promoting ubiquitination and degradation of p21 (Han et al., 2013; Lee et al., 2014). However, the role of RNF114 in CRC metastasis is still unclear.

In this study, we found the mRNA level of XAF1 in mCRC tissues was notably elevated compared with primary tumors, and high XAF1 expression indicated poor prognosis. The mechanistic study revealed that XAF1 acted as a novel adaptor of VCP to promote the deubiquitination and stabilization of the E3 ligase RNF114, which further mediated K48-linked ubiquitination and degradation of JUP. Furthermore, the XAF1–VCP–RNF114–JUP axis promoted CRC metastasis. We also disclosed the correlation between XAF1, RNF114, and JUP in clinical samples. XAF1 is usually considered as a tumor suppressor; however, our study reveals a tumor-promoting effect of XAF1 in mCRC, thus providing a potential therapeutic target for this deadly malignancy.

Results

The expression of XAF1 is associated with the aggressiveness of CRC

To identify potential therapeutic targets for *KRAS*-mutant mCRC, we analyzed the TCGA CRC data to screen the candidates. Gene expression in primary CRC tissues was analyzed, and the standard for the screening is as follows: in *KRAS*-mutant CRC group, gene expression in mCRC patients is higher than that in the patients with non-metastatic CRC, while its expression in mCRC patients is lower or barely changed compared with that in the patients with non-metastatic CRC in *KRAS* wild-type group. According to the above criteria, XAF1 was chosen for further study because the mRNA level of XAF1 was higher in *KRAS*-mutant mCRC patients compared with the patients with non-metastatic CRC, while its expression pattern was opposite in *KRAS* wild-type CRC patients (Fig. 1 A). These results suggested that XAF1 may promote metastasis in *KRAS*-mutant CRC.

To investigate the expression pattern of XAF1 in CRC, we quantified the protein level of XAF1 in 20 pairs of CRC tissues and adjacent normal tissues, including 10 *KRAS* wild-type CRC tissues with the matched normal tissues and 10 *KRAS*-mutant CRC tissues with their matched normal counterparts. Elevated expression of XAF1 was observed in 16 out of 20 CRC tissues compared with the matched normal tissues. The upregulation of XAF1 was more pronounced in the CRC tissues with *KRAS* mutations. Moreover, the expression of XAF1 in *KRAS*-mutant CRC tissues was higher than that in *KRAS* wild-type samples (Fig. 1 B). Upregulation of XAF1 in CRC tissues was further confirmed by immunohistochemistry (IHC; Fig. 1 C). Analysis of the TCGA CRC data also disclosed an increased XAF1 mRNA level in CRC tissues compared with normal samples (Fig. S1 A). Moreover, the tissue microarray results demonstrated that the protein level of XAF1 in the primary CRC tissues in mCRC patients was higher than that in the patients with non-metastatic CRC (Fig. 1 D). In addition, the expression of XAF1 in CRC metastases was significantly higher than that in primary tumors (NCBI GEO accession no. GSE131418-MCC, Fig. 1 E; Kamal et al., 2019). Furthermore, we also found that high expression of XAF1 was associated with poor overall survival in CRC patients (Fig. 1 F). In conclusion, these data suggest a metastasis-promoting potential of XAF1 in CRC.

XAF1 promotes CRC cell migration and metastasis

Based on the significant clinical relevance between XAF1 expression and CRC metastasis, we investigated the effect of XAF1 on CRC cell migration in vitro. First, we ectopically expressed XAF1 in RKO and DLD-1 CRC cells with a low endogenous expression level of XAF1 (Fig. S2 A) and then performed a transwell assay. We found that ectopic expression of XAF1 promoted the migration abilities of RKO and DLD-1 cells (Fig. 2, A and B). Next, we knocked down XAF1 in SW480 and HCT116 cells with high endogenous XAF1 expression and found that depletion of XAF1 remarkably reduced the migration capabilities of SW480 and HCT116 cells (Fig. 2, C and D). To exclude the possibility that XAF1 may influence CRC cell proliferation, MTT assay was employed for validation. As shown in Fig. S2 B, XAF1 exerted a suppressive effect on CRC cell growth only in HCT116 cells. The metastasis-promoting function of XAF1 was further validated in lung metastasis mice model in vivo with luciferase-labeled control and XAF1 knockdown MC38 cells (Chen et al., 2019; Fig. 2, E–H). To interpret the role of XAF1 in *KRAS*-mutant and *KRAS* wild-type CRC cells, we also ectopically expressed XAF1 in *KRAS* wild-type SW48 cells. It was interesting that although XAF1 promoted migration and metastasis of CRC cells with activated KRAS signaling (RKO, DLD-1, SW480, HCT116, and MC38), it had no obvious influence on the migration ability of *KRAS* wild-type SW48 cells (Fig. S2, C and D). This observation was consistent with the analysis of clinical data. Taken together, these data suggest that XAF1 promotes the metastasis of CRC cells both in vitro and in vivo, and this effect might be limited to the cells with activated KRAS signaling.

To explore the mechanism underlying the metastasis-promoting effect of XAF1, we performed RNA sequencing and identified 211 genes that were differentially expressed in XAF1 knockdown SW480 cells using the criteria of fold change >2 and $P < 0.05$ (Fig. S2 E). The GO enrichment analysis revealed that XAF1 significantly influenced cell migration (gene number: 23), cell junction (gene number: 35), and cell adhesion (gene number: 24; Fig. S2, F and G). To confirm the results of RNA-seq, quantitative real-time PCR was performed to examine the expression of the genes in control and XAF1 knockdown SW480 and HCT116 cells. Consistent with the RNA-seq data, the expression of metastasis-promoting genes, including netrin 1 (*NTN1*), secreted protein acidic and cysteine-rich (*SPARC*), extracellular matrix

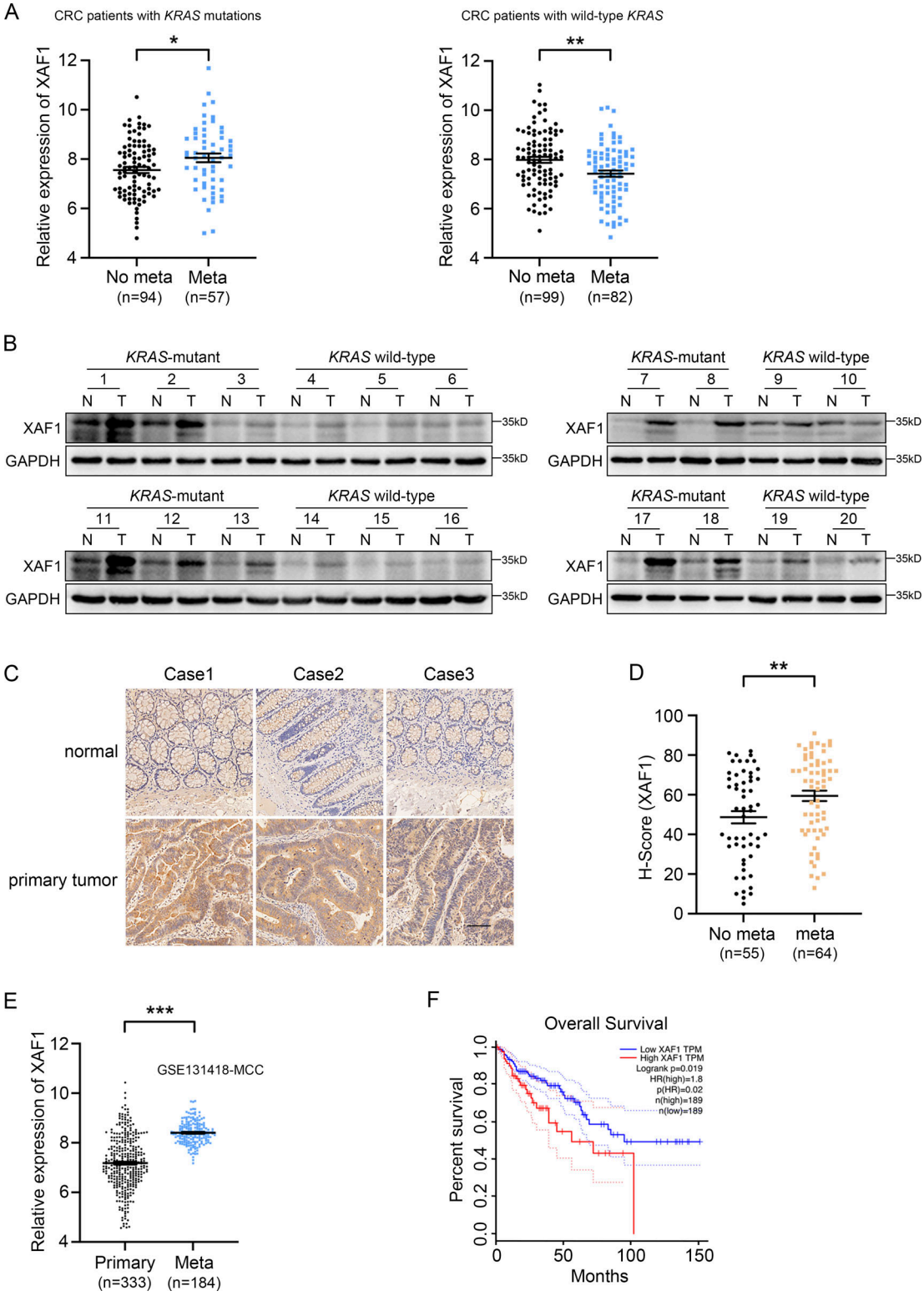

Figure 1. **XAF1 is upregulated in mCRC and high expression of XAF1 indicates poor prognosis. (A)** XAF1 mRNA expression in primary CRC tissues from *KRAS*-mutant and *KRAS* wide-type patients with metastatic or non-metastatic CRC in TCGA COAD dataset. **(B)** XAF1 expression in 20 pairs of normal (N) and the matched CRC tumor (T) tissues was examined by Western blot. **(C)** Representative immunohistochemical staining of XAF1 in paired normal and primary tumor tissues from CRC patients. Scale bar, 200 µm. **(D)** H-scores of XAF1 protein in primary CRC tissues from CRC patients with or without metastasis. **(E)** mRNA expression of XAF1 in primary and metastatic CRC tissues in the GEO dataset (accession no. GSE131418). **(F)** Overall survival of 378 CRC patients with low or high XAF1 expression was analyzed by Kaplan–Meier analysis using the GEPIA web tool. The data in A, D, and E were analyzed by two-tailed unpaired Student's *t* test and represented as the mean ± SEM. *P < 0.05, **P < 0.01, ***P < 0.001. Source data are available for this figure: SourceData F1.

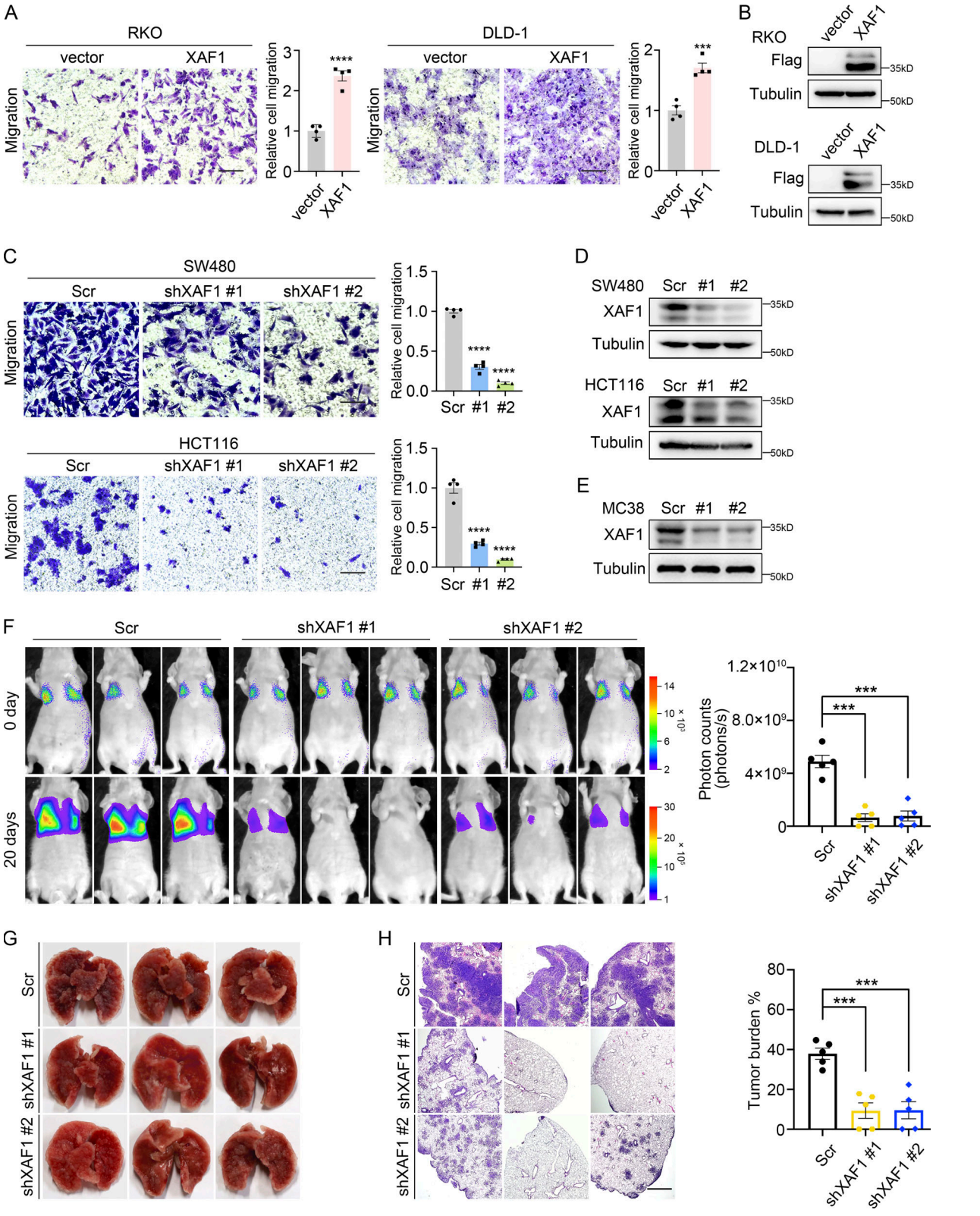

Figure 2. **XAF1 promotes CRC cell migration and metastasis. (A)** Migration capabilities of control and XAF1-overexpressing CRC cells were examined by transwell assay. Left: Representative images. Scale bar, 100 µm. Right: Histograms representing the number of migrated cells relative to control, *n* = 4 random fields. **(C)** Migration abilities of control and XAF1 knockdown CRC cells were assessed by transwell assay. Left: Representative images. Scale bar, 100 µm. Right: Histograms representing the number of migrated cells relative to control, *n* = 4 random fields. Scr, Scramble. **(B and D)** The overexpression (B) and knockdown (D) efficiency of XAF1 in CRC cells were examined by Western blot. Scr, Scramble. **(E)** Western blot showing XAF1 knockdown efficiency in MC38 cells. Scr, Scramble. **(F)** Representative bioluminescent images of the mice in the indicated group and the bioluminescent quantitation of lung metastasis (*n* = 5 mice/

group). Scr, Scramble. **(G)** Representative lung images. Scr, Scramble. **(H)** Representative HE staining of the lung metastatic lesions and the histologic quantification of the lung metastases in the indicated group. The metastatic burden was expressed as the percentage of tumor area in lungs (n = 5 mice/group). Scr, Scramble. Scale bar, 100 μm. The data in A, C, F, and H were analyzed by two-tailed unpaired Student's t test and represented as the mean ± SEM. ***P < 0.001, ****P < 0.0001. Source data are available for this figure: SourceData F2.

protein 1 (*ECM1*), and bone marrow stromal cell antigen 2 (*BST2*), was dramatically decreased in XAF1 knockdown cells (Fig. S2, H and I). Taken together, these data provide further evidence for the metastasis-promoting function of XAF1 in CRC.

XAF1 binds to VCP and RNF114

To explore how XAF1 affects the expression of metastasis-related genes, we utilized mass spectrometry (MS) to analyze the interacting proteins of XAF1. We ectopically expressed 3×Flag-XAF1 in 293T cells and then used Flag beads for coimmunoprecipitation (co-IP), and the immunoprecipitates were further assessed by silver-staining and subsequent MS analysis. Among the candidates, VCP and RNF114 were selected for validation and further study because of their high abundance (Fig. 3 A and Table S1).

We next determined how XAF1 interacted with RNF114 and VCP. XAF1 consists of seven tumor necrosis factor (TNF) receptor-associated factor (TRAF)-like zinc finger (ZF) domains with well-defined domain boundaries (Liston et al., 2001), which contain a highly compact N-terminal domain ($XAF1^{NTD}$), a middle domain ($XAF1^{MD}$), an unstructured linker, and a C-terminal domain ($XAF1^{CTD}$; Tse et al., 2012). Since previous study demonstrates that XAF1 interacts with RNF114 via its C-terminal ZF7 domain (Lee et al., 2014), we constructed a series of XAF1 truncated mutants accordingly and confirmed that XAF1 did interact with RNF114 via its ZF7 domain (Fig. S3 A). Then, we verified the interaction between XAF1 and VCP by both exogenous and endogenous co-IP (Fig. 3, B and C; and Fig. S3 B), GST pull-down (Fig. 3 D), and immunofluorescence (IF) staining (Fig. 3 E). Next, we continued to map the interaction between XAF1 and VCP. As shown in Fig. 3 F, XAF1 bound to VCP via the three N-terminal ZF domains. Furthermore, the interaction between XAF1 and VCP was disrupted by deleting any of the three ZF domains (Fig. S3 C). Based on these observations, we assume that XAF1 might act as an adaptor linking RNF114 and VCP via its C/N-terminal domains.

VCP comprises a N-terminal region, D1 and D2 ATPase domains, and a C-terminal domain (Meyer et al., 2012). VCP regulates distinct pathways by forming multiprotein complexes with specific adaptors (Costantini et al., 2021; Gwon et al., 2021; Turakhiya et al., 2018). The adaptors containing VCP-binding domains, including VBM (VCP-binding motif), VIM (VCP-interacting motif), UBD (ubiquitin-like domain), UBX (ubiquitin regulatory X), UBX-like domain, and SHP box, bind to the N-terminal region of VCP. Other adaptors containing PUL (PLAP [phospholipase A2-activating protein], Ufd3p, and Lub1p) domain, and PUB (PNGase [peptide N-glycosidase]/ubiquitin-associated) domain interact with the C-terminal domain of VCP (Yeung et al., 2008). As shown in Fig. 3 G, XAF1 mainly interacted with the N-terminal region of VCP and also bound to the D1 domain of VCP, although to a much lesser extent. In addition, we aligned the 1–79 residues of XAF1 to the UBX domain of FAF1 and NSFL1C and only found very weak sequence similarities between them (Fig. 3 H), indicating that XAF1 may be a new type of VCP adaptor.

Given that XAF1 interacted with both VCP and RNF114 (Fig. S3 D), we assumed that XAF1 acted as an adaptor linking VCP to RNF114. Consistent with this assumption, RNF114 was found to interact with exogenous VCP (Fig. 3 I), which was further validated by immunofluorescence staining (Fig. 3 J). To examine whether RNF114 formed a ternary complex with XAF1 and VCP, we performed a two-step co-IP assay. As shown in Fig. 3 K, the three molecules formed a ternary complex. Moreover, the knockdown of XAF1 reduced the interaction between VCP and RNF114 (Fig. 3 L), whereas ectopic expression of XAF1 enhanced their association (Fig. S3 E). Ni-NTA pull-down assay verified that XAF1 was necessary for the interaction between VCP and RNF114 in vitro (Fig. S3 F). All these data suggest that XAF1 is a novel adaptor of VCP and facilitates VCP–RNF114 interaction.

XAF1 facilitates the deubiquitination of RNF114 by VCP and YOD1

Since VCP is able to affect the ubiquitination of targeted proteins (Hill et al., 2021; van den Boom and Meyer, 2018), we next determined whether VCP exerted such an effect on RNF114. NMS-873 is a highly selective allosteric inhibitor of VCP (Magnaghi et al., 2013). This inhibitor binds at a cryptic groove in the D2 domain of VCP and interacts with the intersubunit signaling (ISS) motif, preventing its conformational change and thus blocking substrate translocation allosterically (Pan et al., 2021). A previous study using an MS-based proteomics approach has reported that NMS-873 treatment increases the ubiquitination level of 119 proteins (Heidelberger et al., 2018). We analyzed the MS-based proteomics dataset and found that the ubiquitination level of RNF114 was increased upon NMS-873 treatment (Fig. S4 A), indicating that VCP may affect the ubiquitination status of RNF114.

Since VCP and RNF114 existed in a complex and VCP inhibitor elevates the ubiquitination level of RNF114, we wondered whether VCP could affect the protein level of RNF114. We constructed VCP-depleted SW480 and HCT116 cells and examined the protein expression of RNF114. As shown in Fig. 4 A, VCP depletion apparently declined the protein level of RNF114. Furthermore, the expression of endogenous RNF114 was decreased upon NMS-873 treatment in a dose-dependent manner in several CRC cells (Fig. 4, B and C; and Fig. S4 B), whereas NMS-873 treatment did not affect the protein level of XAF1 (Fig. 4 C). Additionally, the effect of NMS-873 on RNF114 was severely weakened in XAF1 knockdown cells (Fig. 4 C), suggesting that XAF1 was required for the regulation of RNF114 by VCP. Next, we examined the influence of VCP on the ubiquitination status of RNF114. We found that wild-type VCP, but not R95G mutant

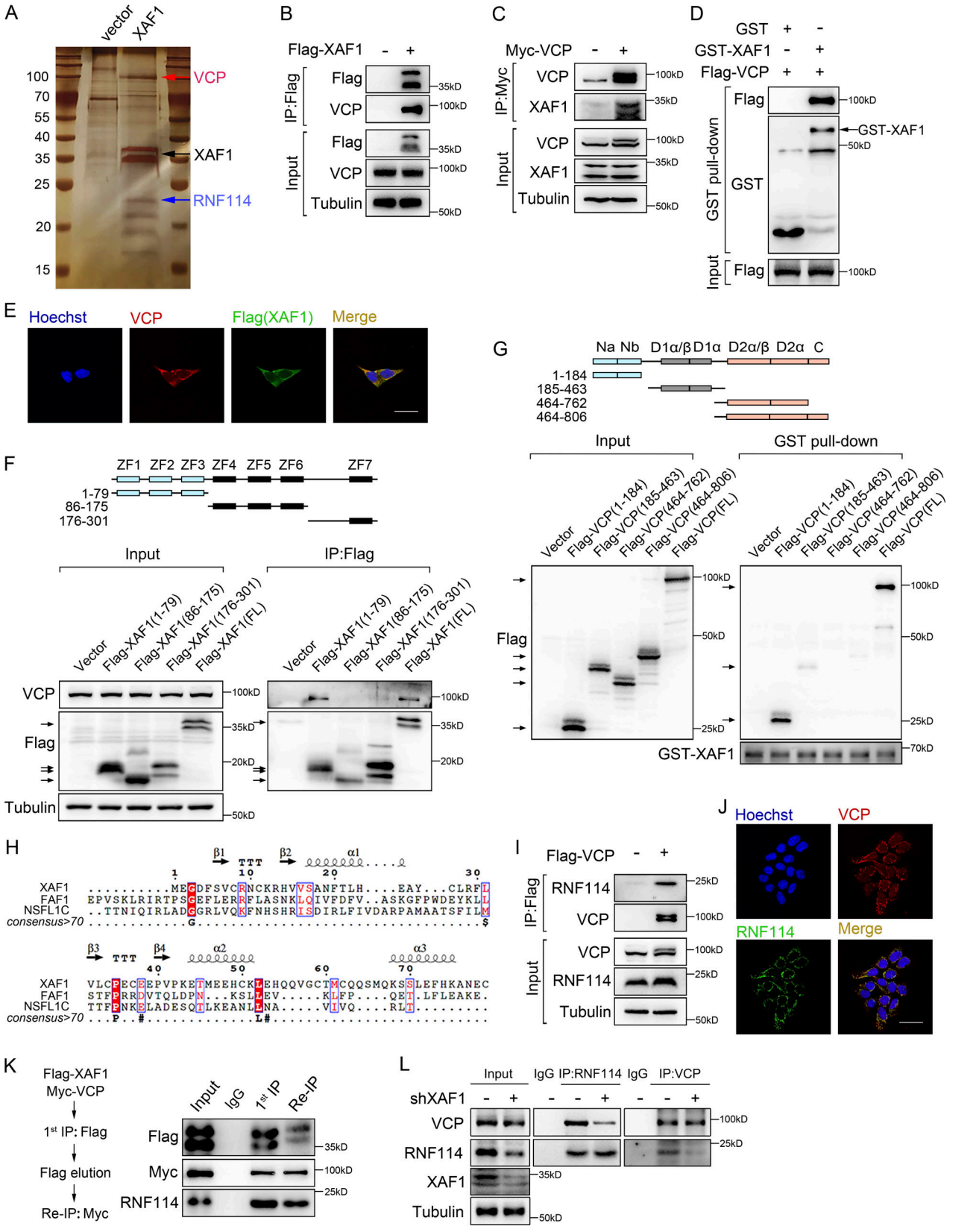

Figure 3. **XAF1 facilitates the interaction between VCP and RNF114. (A)** Silver-stained gel showing differential bands between control and XAF1-overexpressing samples. **(B–D)** The interaction between XAF1 and VCP was examined by co-IP assay (B and C) and GST pull-down assay (D). **(E)** Co-localization of VCP and XAF1 (Flag-tagged) in XAF1-overexpressing DLD-1 cells. Scale bar, 45 μm. **(F)** Co-IP assay was performed to map the interactions between VCP and XAF1 in 293T cells. **(G)** GST pull-down assay was used to assess the interaction between truncated VCP mutants and purified GST-XAF1 protein. **(H)** Clustal-based sequence alignment of the VCP-binding site within XAF1 and UBX domain within FAF1 and NSFL1C. Secondary structure elements of

the 1–79 residues of XAF1 calculated by Phyre2 were shown above the alignment. **(I)** Co-IP assay showing the interaction between RNF114 and VCP. **(J)** Co-localization of VCP and RNF114 protein in DLD-1 cells was examined by IF. Scale bar, 45 μm. **(K)** Two-step co-IP assay was performed to identify the complex containing XAF1, VCP, and RNF114. IgG was used as a negative control. **(L)** The interaction between VCP and RNF114 in control and XAF1 knockdown cells was examined by co-IP. IgG was used as a negative control. Source data are available for this figure: SourceData F3.

(Tang et al., 2010; Weihl et al., 2006), could effectively reduce the ubiquitination level of RNF114 (Fig. 4 D). To clarify the role of XAF1 in the regulation of RNF114 by VCP, we employed NMS-873 to treat control, XAF1 knockdown, and XAF1-overexpressing cells. We found that RNF114 ubiquitination was elevated upon VCP inhibition and XAF1 knockdown, and the latter exhibited a stronger effect (Fig. 4 E), which was consistent with the alteration of RNF114 shown in Fig. 4 C. In contrast, ectopic expression of XAF1 diminished the ubiquitination of RNF114. However, this effect was abolished by NMS-873 (Fig. 4 F). These data were in accordance with the "VCP-adaptor (XAF1)-substrate (RNF114)" model. Taken together, these data suggest that XAF1 and VCP cooperatively regulate the deubiquitination and stability of RNF114.

Previous studies have reported that VCP complexes contain deubiquitinases such as YOD1 (Ernst et al., 2009), Ataxin 3 (ATX3; Arrojo E Drigo et al., 2013), and VCPIP1 (Zhang and Wang, 2015). To find out the deubiquitinating enzyme of RNF114, we knocked down these molecules respectively in control and XAF1-overexpressing DLD-1 cells. Among the three deubiquitinases, only YOD1 depletion led to the downregulation of RNF114 (Fig. S4, C–E). Moreover, the interaction between RNF114 and YOD1 was verified by GST pull-down assay (Fig. 4 G). YOD1 knockdown remarkably promoted the ubiquitination of RNF114. In addition, XAF1 overexpression reduced the ubiquitination of RNF114; however, this effect was abolished by YOD1 depletion (Fig. 4 H). These data suggest that YOD1 is a deubiquitinase of RNF114 in VCP complex.

The migration-promoting effect of XAF1 depends on RNF114

To explore the role of RNF114 in XAF1-regulated CRC cell migration, we knocked down RNF114 to examine its influence on cell migration. We found that the knockdown of endogenous RNF114 in SW480 and HCT116 cells significantly reduced the migration abilities of CRC cells compared with control (Fig. S4, F and G), suggesting that RNF114 could regulate CRC cell migration in vitro.

To address whether RNF114 was necessary for XAF1-promoted migration of CRC cells, we knocked down RNF114 in control and XAF1-overexpressing DLD-1 cells (Fig. 4 I) and found that the migration-promoting effect of XAF1 was significantly abolished by RNF114 depletion (Fig. 4 J). Therefore, these data suggest that RNF114 mediates the migration-promoting effect of XAF1.

JUP is a substrate for E3 ligase RNF114

Previous studies suggest that RNF114 modulates cancer metastasis by exerting its E3 ligase activity toward substrates like PARP10 (Zhao et al., 2021) and EGR1 (Feng et al., 2022). Hence, we explored the substrates of RNF114 in CRC by MS analysis of RNF114-interacting proteins and identified JUP as a putative substrate for RNF114 (Fig. 5 A and Table S2). Consistently, the interaction between JUP and RNF114 was confirmed by both exogenous and endogenous co-IP (Fig. 5, B and C).

JUP, also known as γ-catenin, is a member of the armadillo family of proteins and a paralog of β-catenin (Chen et al., 2020). JUP acts as a component of both desmosome and adherens junctions, linking cadherins to the cytoskeleton (Li et al., 2011). Additionally, JUP participates in signal transduction like its homolog β-catenin (Aktary et al., 2017). To examine whether JUP was a substrate of RNF114, wild-type and C44W/C49W mutant RNF114, which has impaired ubiquitin ligase activity (Yang et al., 2017), were ectopically expressed in 293T cells, respectively. We found that the ectopic expression of wild-type RNF114, but not C44W/C49W mutant, dramatically increased the ubiquitination level of JUP (Fig. 5 D) and reduced its protein level (Fig. S5 A). By contrast, as shown in Fig. 5 E, the ubiquitination level of JUP was remarkably decreased in RNF114 knockdown cells compared with that in control cells. Taken together, these data suggest that JUP is a novel substrate of RNF114.

Ubiquitination is one of the most prevalent posttranslational modifications (PTMs), regulating different cellular processes. Lys-48(K48)-linked ubiquitination usually leads to proteasomal degradation, while Lys-63(K63)-linked ubiquitination is involved in cellular signaling transduction (van Wijk et al., 2019). We examined the type of ubiquitin chains on JUP by using K48-/K63-linkage specific antibodies or constructs expressing K48-/K63-only ubiquitin mutants in control, RNF114-overexpressing and RNF114 knockdown cells, and found that RNF114 mediated K48-linked ubiquitination of JUP (Fig. 5 F and Fig. S5 B). Consistently, RNF114 knockdown upregulated JUP expression (Fig. 5 G), and depletion of XAF1 led to downregulation of RNF114 and elevated expression of JUP (Fig. 5 H). Accordingly, RNF114 knockdown notably increased the protein stability of endogenous JUP (Fig. S5 C), and XAF1 knockdown retarded the decline of JUP upon cycloheximide treatment (Fig. S5 D). Furthermore, there was a significant negative correlation between the expression of XAF1 and JUP in CRC cells with activated KRAS signaling (Fig. S5 E). IF staining also demonstrated that RNF114 knockdown resulted in JUP accumulation, whereas ectopic expression of RNF114 or XAF1 reduced the expression of JUP (Fig. 5 I). Therefore, our data suggest that XAF1 promotes CRC cell migration by stabilizing RNF114, which leads to the degradation of the cell–cell junction protein JUP.

XAF1 promotes CRC metastasis by downregulating JUP

Since JUP is an essential molecule in cell adhesion, we investigated whether XAF1 and JUP affected cell adhesion using a dispase-based dissociation assay and DiD-labeled cell adhesion assay. We observed that XAF1 depletion promoted intercellular adhesion, whereas JUP knockdown decreased cell–cell adhesion in SW480 cells (Fig. S5, F and G). Since cell–cell adhesion molecules play a significant role in cancer metastasis, we examined

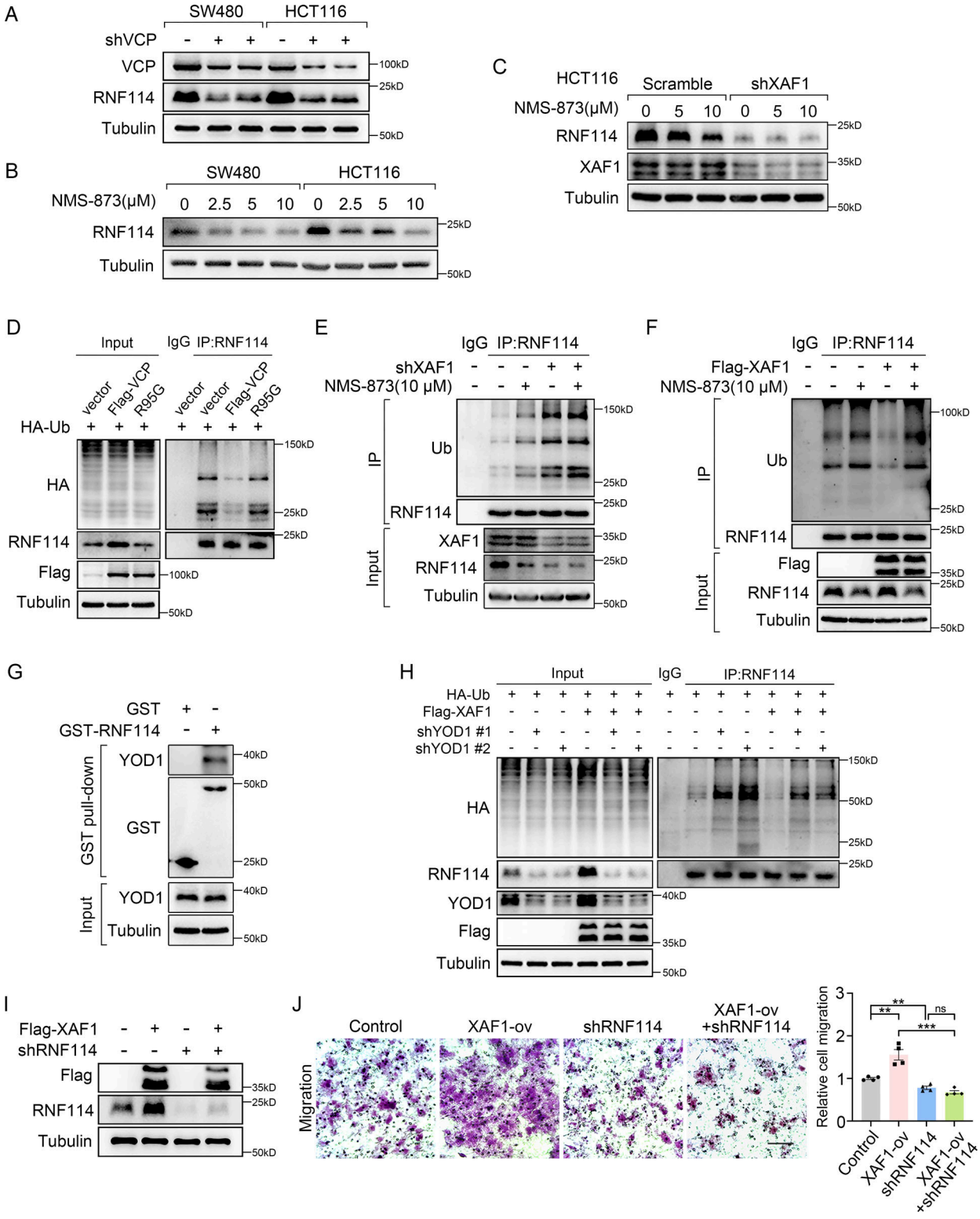

Figure 4. **XAF1 is required for VCP-mediated deubiquitination of RNF114. (A)** The protein level of RNF114 in control and VCP-depleted SW480 and HCT116 cells was assessed by Western blot. **(B)** Western blot showing the influence of NMS-873 on RNF114 in CRC cells. Cells were treated with NMS-873 for 8 h. **(C)** The influence of NMS-873 on RNF114 in control and XAF1 knockdown HCT116 cells was examined by Western blot. Cells were treated with NMS-873 for 8 h. **(D)** The ubiquitination of RNF114 was examined in 293T cells transfected with vector, wild-type, and mutant VCP, respectively. IgG was used as a negative control. **(E)** The ubiquitination of RNF114 was examined in control and XAF1 knockdown MC38 cells. Cells were treated with 10 μM NMS-873 for 8 h. IgG was used as a negative control. **(F)** The ubiquitination of RNF114 was examined in control and XAF1-overexpressing 293T cells. Cells were treated with 10 μM NMS-873 for 8 h. IgG was used as a negative control. **(G)** The interaction between RNF114 and YOD1 was examined by GST pull-down assay. **(H)** The ubiquitination of RNF114 was examined in control, XAF1-overexpressing, YOD1 knockdown, and XAF1-overexpressing + YOD1 knockdown DLD-1 cells. IgG was

used as a negative control. **(I)** Western blot showing the XAF1 overexpression and RNF114 knockdown efficiency in DLD-1 cells. **(J)** Cell migration was examined in control, XAF1-overexpressing, RNF114 knockdown, and XAF1-overexpressing + RNF114 knockdown DLD-1 cells. Left: Representative images. Scale bar, 100 µm. Right: Histograms representing the number of migrated cells relative to control, $n = 4$ random fields. The data in J were analyzed with one-way ANOVA with Bonferroni post-hoc multiple comparison test and represented as the mean ± SEM. ns: not significant, **P < 0.01, ***P < 0.001. Source data are available for this figure: SourceData F4.

the role of JUP in XAF1-promoted metastasis. We first tested this hypothesis by transwell assay and found that JUP knockdown significantly rescued the decreased cell migration caused by XAF1 depletion in CRC cells (Fig. 6, A and B).

Next, we labeled the XAF1-, JUP-, both XAF1- and JUP-depleted, and control CRC cells with luciferase and measured the lung metastasis in vivo (Chen et al., 2019). Consistent with the phenotype in vitro, XAF1 knockdown reduced lung metastasis of CRC cells and the nude mice injected with XAF1-deficient MC38 cells showed fewer lung metastasis than control. The reduced metastasis caused by XAF1 deficiency could be largely rescued by JUP knockdown (Fig. 6, C and D). In summary, the in vitro and in vivo data indicate that JUP acts as a negative mediator of XAF1-regulated metastasis.

Correlations between XAF1, RNF114, and JUP in clinical samples

The above data suggest that the XAF1–RNF114–JUP axis might be a potential therapeutic target for mCRC. Therefore, we explored the expression pattern of XAF1, RNF114, and JUP in clinical samples. IHC staining of the three molecules in CRC tissue microarray revealed elevated protein levels of XAF1 and RNF114 (Fig. 7, A and B), and reduced protein levels of JUP in CRC samples compared with the matched normal counterparts (Fig. 7 C). Statistical analysis revealed a positive correlation between XAF1 and RNF114 and negative correlations between RNF114 and JUP, XAF1 and JUP, respectively, in clinical samples (Fig. 7, D–G).

According to the scores of XAF1 staining intensity in the tissue microarray, we divided the patients into XAF1-low (H score ≤40) and -high (H score >40) groups, and the relationship between XAF1 expression and clinical pathology features was assessed (Table S3). XAF1 expression was positively correlated with tumor metastasis and pathological grade. The clinical data is consistent with our conclusion, suggesting that XAF1 is a metastasis promoter in CRC.

Discussion

In this study, we found that XAF1 was frequently elevated in mCRC tissues compared with primary counterparts, and higher XAF1 was associated with poorer overall survival of CRC patients. Previous studies of XAF1 mainly focus on its proapoptotic effect as a tumor suppressor. For instance, XAF1 directs the apoptotic switch of p53 signaling through activation of HIPK2 and RNF114 (Lee et al., 2014). In addition, XAF1 forms a positive feedback loop with IRF-1 to stabilize and activate IRF-1 to suppress tumorigenesis under stressful conditions (Jeong et al., 2018). Different from the previous reports, we found that XAF1 had tumor-promoting properties, suggesting that the role of XAF1 in cancer may be stage- and context-dependent.

Moreover, we identified XAF1 as a novel type of VCP adaptor. VCP regulates numerous substrates with the assistance of diverse adaptors, and distinct adaptors of VCP participate in different cellular processes. The most extensively studied adaptors possess the UBX/UBX-like domains or the ubiquitin-associated (UBA) domains. Beyond that, some adaptors possess other VCP-binding domains, such as PUB and PUL (Yeung et al., 2008). We found that the 1–79 residues of XAF1 represented a new type of VCP-binding domain interacting with the N-terminal region of VCP. Furthermore, XAF1 binds to RNF114 via its C-terminal ZF7 domain. These interactions make it suitable for XAF1 to function as a VCP adaptor protein to regulate the deubiquitination and stability of RNF114. It is reported that XAF1 interacts with ER stress sensor glucose-regulated protein (GRP78) via the C-terminal region, leading to the degradation of GRP78 in an RNF114-dependent manner (Lee et al., 2022). XAF1 interacts with ERα and BRCA1 via the ZF domains 5/6 and 4, respectively, and destabilizes ERα through the assembly of BRCA1-mediated destruction complex and promotes estrogen-induced apoptosis (Lim et al., 2022). XAF1–XIAP axis regulates the activity and stability of KLHL22 through a ubiquitin-dependent way, and thus controls IRF7 protein abundance and helps maintain proper IFN-I production (Liu et al., 2023). In addition, XAF1 binds to and regulates the ubiquitination of IRF-1 via the ZF6 domain (Jeong et al., 2018). XAF1 interacts with p53, Siah2, and RNF114 via the ZF5, ZF6, and ZF7 domain, respectively, and the regulation of p53 signaling by XAF1 results from the cooperative function of these domains (Lee et al., 2014). Thus, our study expanded the understanding of XAF1 in the regulation of protein ubiquitination and stability.

RNF114 has been shown to take part in the regulation of cell cycle and metastasis, but the impact of RNF114 on CRC migration and metastasis has not been reported. In the current study, we reported the elevated expression of RNF114 in CRC tissues compared with normal counterparts. The mechanistic study identified RNF114 as a new substrate of VCP and verified JUP as a substrate for RNF114. JUP, a component of both desmosome and adherens junctions, restrains tumor metastasis in breast cancer (Bailey et al., 2012), gastric cancer (Chen et al., 2020), renal cell carcinoma (Chen et al., 2021), and lung adenocarcinoma (Hao et al., 2018). Previous studies have shown that FBW7 regulates JUP function via K63-linked ubiquitination (Li et al., 2018). Here, we demonstrated that RNF114 promoted K48-linked ubiquitination of JUP, which accelerated the degradation of JUP and CRC metastasis. Moreover, we observed a positive correlation between XAF1 and RNF114, and negative correlations between JUP and XAF1, JUP and RNF114 in CRC clinical samples, which further proved the involvement of XAF1–RNF114–JUP axis in CRC aggressiveness.

In conclusion, our study reveals the metastasis-promoting effect of XAF1 and the underlying mechanism in CRC (Fig. 7 H), providing a diagnostic biomarker and potential therapeutic target for mCRC.

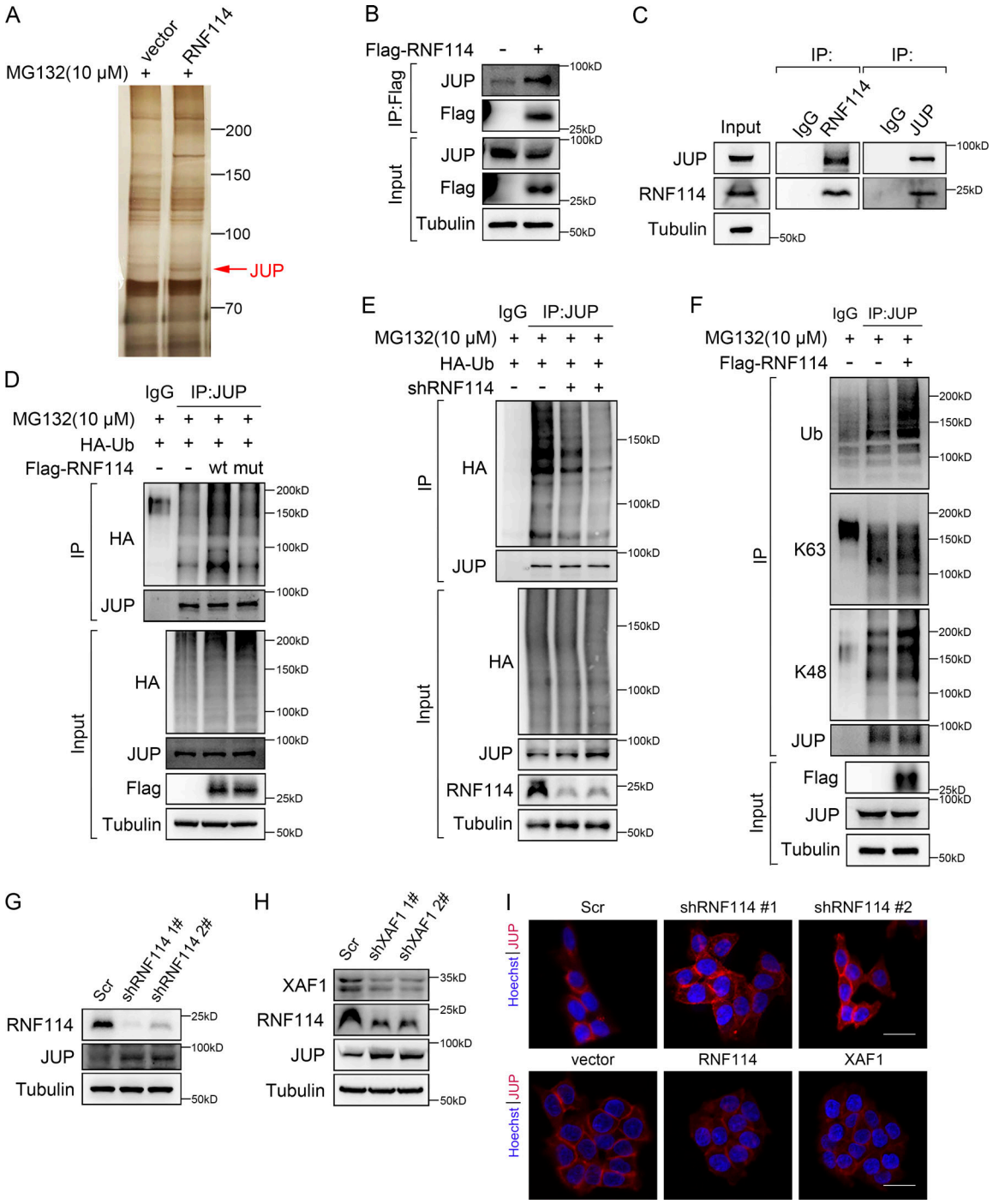

Figure 5. **Identification of JUP as a substrate of RNF114. (A)** Silver-stained gel showing differential bands between control and RNF114-overexpressing samples. Cells were treated with 10 μM MG132 for 8 h. **(B and C)** The interaction between RNF114 and JUP was examined by co-IP assay. IgG was used as a negative control. **(D)** The ubiquitination of JUP was examined in 293T cells transfected with vector, wild-type, and mutant RNF114, respectively. Cells were treated with 10 μM MG132 for 8 h. IgG was used as a negative control. **(E)** The ubiquitination of JUP was examined in control and RNF114-depleted HCT116 cells. Cells were treated with 10 μM MG132 for 8 h. IgG was used as a negative control. **(F)** Co-IP was performed to detect the types of ubiquitin chains on JUP. Cells were treated with 10 μM MG132 for 8 h. IgG was used as a negative control. **(G)** Western blot showing JUP protein level in control and RNF114 knockdown HCT116 cells. Scr, Scramble. **(H)** Protein levels of RNF114 and JUP in control and XAF1 knockdown HCT116 cells. Scr, Scramble. **(I)** Immunofluorescence staining showing JUP expression in control and RNF114 knockdown HCT116 cells (upper), and control, RNF114/XAF1-overexpressing HCT116 cells (lower). Scr, Scramble, Scale bar, 45 μm. Source data are available for this figure: SourceData F5.

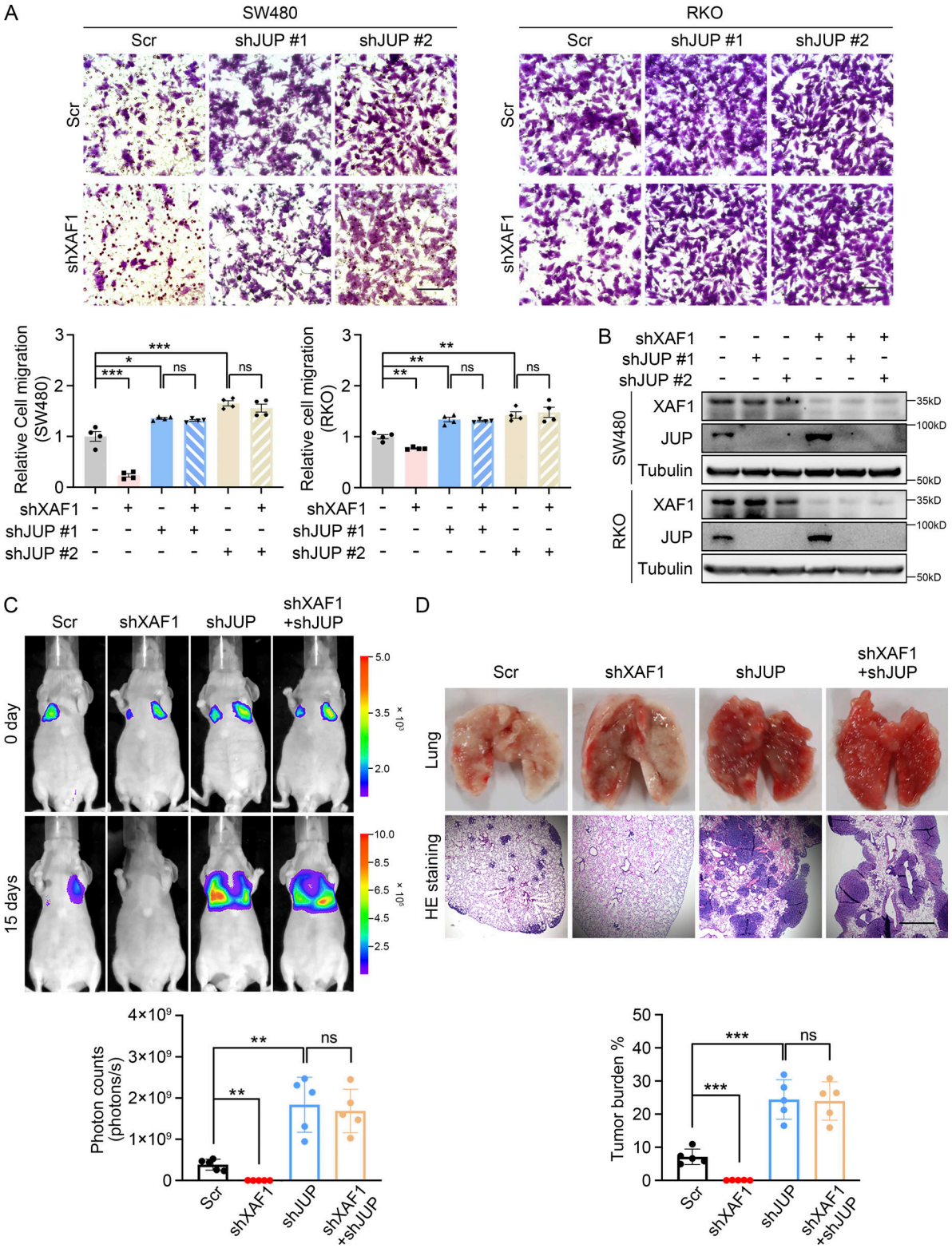

Figure 6. **XAF1 promotes CRC metastasis by downregulating JUP. (A)** Migration capabilities of control, XAF1 knockdown, JUP knockdown, and XAF1/JUP double knockdown SW480 and RKO cells were examined by transwell assay. Upper: Representative images. Scale bar, 100 μm. Lower: Histograms representing the number of migrated cells relative to control, *n* = 4 random fields. Scr, Scramble. **(B)** Western blot showing XAF1/JUP knockdown efficiency. **(C)** Representative bioluminescent images of mice in the indicated group (upper) and the bioluminescent quantitation of lung metastasis (*n* = 5 mice/group) (lower). Scr, Scramble. **(D)** Representative lung images and HE staining of the lung metastatic lesions (upper), and the histologic quantification of the lung metastases in the indicated group. The metastatic burden was expressed as the percentage of tumor area in lungs (*n* = 5 mice/group). Scr, Scramble. Scale bar, 100 μm. The data in A, C, and D were analyzed with one-way ANOVA with Bonferroni post-hoc multiple comparison test and represented as the mean ± SEM. ns: not significant, *P < 0.05, **P < 0.01, ***P < 0.001. Source data are available for this figure: SourceData F6.

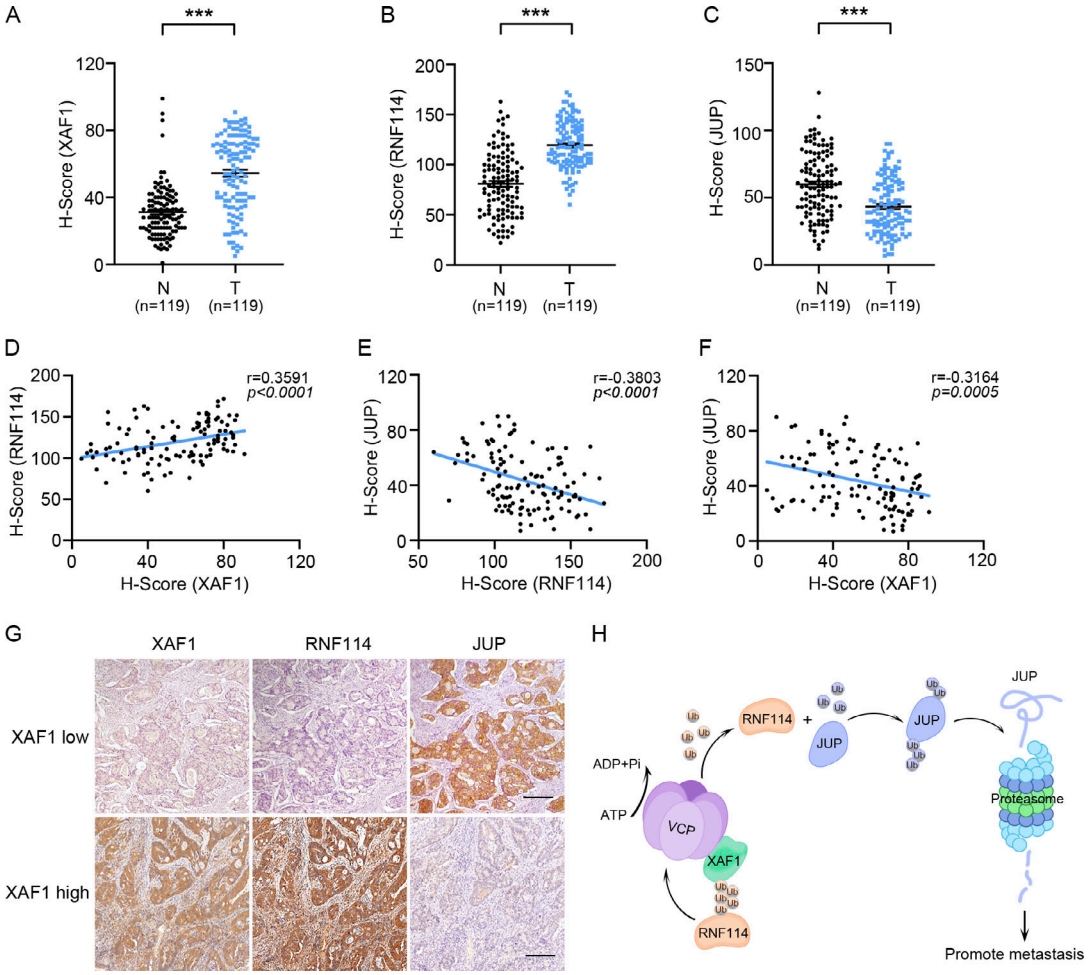

Figure 7. **Significant correlations between XAF1, RNF114, and JUP in clinical CRC samples. (A–C)** H-scores of XAF1 (A), RNF114 (B), and JUP (C) in 119 pairs of CRC and the adjacent normal tissues. **(D–F)** The correlations between the expression of XAF1 and RNF114 (D), RNF114 and JUP (E), and XAF1 and JUP (F) in the tumor tissues from 119 CRC patients were analyzed by Pearson correlation analysis. **(G)** Representative immunohistochemical staining images of XAF1, RNF114, and JUP in the similar regions within serial tumor sections from CRC patients. Scale bar, 200 μm. **(H)** Schematic representation demonstrating the molecular mechanism underlying the metastasis-promoting effect of XAF1 in CRC. The data in A–C were analyzed by two-tailed unpaired Student's *t* test and represented as the mean ± SEM. ***P <0.001.

Materials and methods

Cell culture

HEK293T and CRC cells were purchased from the Type Culture Collection of the Chinese Academy of Sciences. DLD-1 cells were cultured in RPMI-1640 (Gibco) supplemented with 10% fetal bovine serum (FBS; Anlite) and 1% penicillin–streptomycin (Sangon Biotech). Except for DLD-1, all the other cell lines were cultured in DMEM (Gibco). Cells were incubated at 37°C in a humidified 5% CO_2 atmosphere. All cells were frozen and stored in liquid nitrogen before experimentation. Cells were brought into culture for no more than 4 wk. Mycoplasma testing was performed approximately every 3 mo on all cells in use at the time using MycAway Plus-Color One-Step Mycoplasma Detection Kit from Yeasen Biotechnology.

Human tumor samples

After obtaining written informed consent, all CRC and paired adjacent tissues were collected at the Hangzhou First People's Hospital, in compliance with the protocol for tissue collection approved by the Ethics Committee. All experiments were approved by the Ethical Committee. Detailed pathological examination parameters were recorded and available for analysis.

Plasmid constructs

XAF1 and VCP coding sequences were inserted into the p23-3×Flag-GFP lentiviral vector. XAF1 and RNF114 coding sequences were inserted into the pGEX-4T-1 vector. VCP coding sequence was inserted into the pET-28a vector. Wild-type and C44W/C49W mutant RNF114 were cloned into the p23-3×Flag-GFP vector, respectively. VCP R95G mutation was cloned into the p23-3×Flag-GFP vector. shRNAs targeting XAF1, RNF114, VCP, and JUP were inserted into pLKO.1-TRC vector. The sequences of the primers for gene cloning and shRNAs are listed in Table S4 and Table S5, respectively.

RNA-seq analysis of transcriptome

Total RNA was extracted separately from Scramble and XAF1 knockdown SW480 cells using TRIzol reagent (Invitrogen).

After cDNA library construction, the samples were sequenced using the Illumina Novaseq 6000 platform. DEGs were screened by DESeq under the criteria of $|\log_2 FC| \geq 1$ and P adjust <0.05. GO enrichment analysis was performed using Goatools. These data were analyzed on the online platform of Majorbio Cloud Platform (http://www.majorbio.com).

qPCR

Total mRNA was isolated from cultured cells using TRIzol reagent (Invitrogen), according to the manufacturer's instructions. 2 μg of total RNA was reverse transcribed into cDNA using M-MLV Reverse Transcriptase (Promega) according to the manufacturer's protocol. SYBR Green Kit (YEASEN Biotech) was applied to quantify PCR amplification. Gene expression levels were calculated using the ΔCT-method. The primer pairs used in our study are described in Table S6.

Western blot

Cells were scraped and lysed in RIPA buffer (50 mM Tris [pH 7.4], 150 mM NaCl, 1% Triton X-100, and 1% sodium deoxycholate) with protease inhibitors and phosphatase inhibitors, then the lysates were centrifuged at 14,000 rpm (4°C for 15 min). Protein concentrations were determined using the Bradford reagent according to the manufacturer's instructions. After boiling for 5 min with 6 × loading buffer, proteins were separated using 8% and 12% SDS-PAGE gels and then transferred to PVDF membranes (0.45 μm). Then the PVDF membrane was cropped to facilitate the examination of the target proteins with different molecular weights in the same sample. When the membrane was cropped, the margin was kept as wide as possible. The cropped membranes were blocked in 5% BSA. After blocking, the membranes were incubated with primary antibodies at 4°C overnight, washed three times with TBST, and then incubated with the mouse/rabbit secondary antibodies for 60 min at room temperature. The primary antibodies used in our study are described in Table S7. Horseradish peroxidase-conjugated secondary antibodies (1:2,000) were purchased from Cell Signaling Technology. The Western blot images were obtained with uniform size (2.91 × 2.34 cm, 600 dpi) by Tanon 5200 Chemiluminescent Imaging System. The unprocessed images of the blots were provided in source data documents. In many cases, the blots were cut prior to incubation with the antibody. Sometimes, the signal of the blots was so strong that the exposure time was very short, resulting in a bright background that obscured the edges of the blots. Therefore, the edges of these blots (determined by the images with longer exposure time or the bright field images) were marked with a blue dotted box in the source data documents.

GST fusion protein purification and GST pull-down assay

GST, GST-XAF1, and GST-RNF114 proteins were purified from BL21 bacteria according to the manual. Briefly, coding sequences were subcloned into the pGEX-4T-1 vector. Vectors were transformed into BL21 bacteria. Bacteria were cultured in an LB medium with ampicillin until the culture reached an optical density of 0.8 at 600 nm (OD_{600}). IPTG was added to a final concentration of 0.5 mM; afterward, the incubation was continued overnight at 16°C. Cells were pelleted down and resuspended in PBS with protease inhibitor. They were sonicated for 30 min and incubated with 1% Triton X-100 for another 30 min, followed by centrifuging at 12,000 rpm for 20 min at 4°C. The supernatant was incubated with glutathione sepharose 4B (GE) for 2 h at 4°C. The beads were pelleted down and washed five times with PBS. Then the GST fusion proteins were eluted with 10 mM reduced glutathione. The purified proteins were condensed by Amicon Ultra Centrifugal Filter Unit (Millipore) according to the manufacturer's instructions. To purify untagged XAF1 protein, the beads were incubated with thrombin for 16 h at 4°C. After centrifuging, the supernatant was condensed as described above. Bradford reagent was used to determine the concentration of the purified protein.

For the GST pull-down assay, the lysate of cultured cells was incubated with 10 μg GST or GST fusion protein overnight at 4°C. On the second day, the mixture was incubated with glutathione sepharose 4B for 2 h at 4°C and then the GST beads were washed three times and analyzed by Western blot with the indicated antibodies.

His fusion protein purification and Ni-NTA pull-down assay

His-VCP was purified from BL21 bacteria according to the manual. Briefly, coding sequences were subcloned into the pET-28a vector. Vectors were transformed into BL21 bacteria. Bacteria were cultured in LB medium with kanamycin until the culture reached an optical density of 0.8 at 600 nm (OD_{600}). IPTG was added to a final concentration of 0.1 mM, afterward, the incubation was continued overnight at 16°C. Cells were collected by centrifuging for 5 min at 6,000 rpm, resuspended in binding buffer (5 mM imidazole, 300 mM NaCl, and 20 mM Na_2HPO_4, pH 7.8) with protein inhibitor, then sonicated for 30 min, and incubated with 1% Triton X-100 for another 30 min. Afterward, the cells were incubated with Ni-NTA Agarose (Qiagen) for 2 h at 4°C. The beads were pelleted down and washed five times with wash buffer (25 mM imidazole, 300 mM NaCl, and 20 mM Na_2HPO_4, pH 7.8). The His-tagged proteins were eluted by an elution buffer (250 mM imidazole, 300 mM NaCl, and 20 mM Na_2HPO_4, pH 7.8). The purified proteins were condensed by Amicon Ultra Centrifugal Filter Unit (Millipore) according to the manufacturer's instructions. Bradford reagent was used to determine the concentration of the purified protein.

For Ni-NTA pull-down assay, His-tagged VCP was incubated with GST-tagged RNF114 in the absence or presence of the untagged XAF1 overnight at 4°C. On the second day, the protein solution was incubated with Ni-NTA Agarose for 2 h at 4°C. Afterward, the Ni-NTA Agarose was washed three times and then analyzed by Western blot with the indicated antibodies.

Immunoprecipitation

Cells were lysed in IP lysis buffer (50 mM Tris-HCl, pH 7.4 with 150 mM NaCl, 1 mM EDTA, and 1% Triton X-100) with protease inhibitors and phosphatase inhibitors. The cell extracts were then incubated with the corresponding primary antibody overnight at 4°C. Protein A/G Sepharose beads were added and further incubated for another 4 h at 4°C. Afterward, the beads were washed three times with ice-cold IP lysis buffer and boiled

for 10 min in 40 µl 2 × loading buffer and then subjected to Western blot analysis.

IHC

Paraffin-embedded tissue sections were deparaffinized, rehydrated, and subjected to antigen retrieval. Subsequently, the endogenous peroxidase activity of sections was blocked with 3% H_2O_2 in methanol. After washing with 0.01 M PBS (15 mM NaCl, 8 mM Na_2HPO_4, and 2 mM NaH_2PO_4) three times, the sections were blocked by 0.01 M PBS supplemented with 5% normal goat serum and 0.3% Triton X-100. Next, sections were incubated with primary antibodies against XAF1 (1:100; Affinity), RNF114 (1:100; Absci), and JUP (1:50; Cell Signaling Technology), respectively, overnight at 4°C. After washing with 0.01 M PBS three times, the sections were incubated with a secondary antibody (1:500) for 2 h. After washing once with 0.01 M PBS and twice with 0.05 M Tris-HCl (pH = 7.6) solution, the sections were visualized with 0.03% 3,3′-diaminobenzidine in 0.05 M Tris-HCl (pH 7.6) and counterstained with hematoxylin. Images were captured at room temperature using Echo Revolve Hybrid Microscope (Echo) using 20 × objective at bright field mode. The extent and staining intensity of protein were scored automatically by Vectra 2 system (PerkinElmer).

IF

Cells plated on slides were washed three times with PBS buffer and fixed with 4% PFA in PBS for 15 min at 37°C. Cells were then blocked with PBS containing 5% bovine serum albumin for 1 h at 37°C and incubated with primary antibodies against VCP (1:100; Proteintech), RNF114 (1:100; Absci), JUP (1:100; Cell Signaling Technology), and Flag (1:500; Sigma-Aldrich) overnight at 4°C. After three washes with PBS, the cells were incubated with a secondary antibody (Alexa Fluor 488-conjugated donkey anti-mouse IgG, 1:1,000; Alexa Fluor 555-conjugated donkey anti-rabbit IgG, 1:1,000) for 1.5 h at room temperature and washed three times with PBS. The nuclei were stained with Hoechst dye. Fluorescence images were captured at room temperature using an inverted confocal laser scanning microscope Zeiss LSM880 (Carl Zeiss) with 63 × oil objective. Images were acquired using ZEN software (Carl Zeiss).

Mass spectrometry analysis

293T cells overexpressing Flag-tagged XAF1, Flag-tagged RNF114, and control cells were lysed followed by immunoprecipitation with the anti-FLAG M2 Agarose (Sigma-Aldrich) according to the immunoprecipitation assay protocol. The bound proteins were eluted by competition with a large excess of free FLAG peptide, then the elution fractions were separated by SDS-PAGE gels and the protein bands were visualized by silver staining (Beyotime Biotechnology) according to the manufacturer's instructions. The subsequent mass spectrometry analyses were performed by Shanghai Applied Protein Technology Co. Ltd.

Transwell assay

Transwell assay was performed in 24-well inserts (8.0 µm; Corning). Briefly, 5 × 10^5 cells suspended in 200 µl serum-free medium were loaded on the top, and 500 µl complete medium was placed into the bottom side. 48 h later, the migrated cells were stained with 0.1% crystal violet. Images were captured at room temperature using Echo Revolve Hybrid Microscope (Echo) using a 10× objective at brightfield mode. Cells were counted using ImageJ software and the data were presented as the mean ± SEM., calculated from four randomly selected fields.

Dispase-based dissociation assay

2 × 10^6 cells were seeded onto six-well plates. After 24 h, cell monolayers were washed twice in PBS and then incubated in 1 ml of dispase (2.4 U/ml; Sigma-Aldrich) for 30 min at 37°C until the cell monolayer detached from the well bottom. Defined mechanical stress was applied with an electrical pipette. Images for fragment counting were taken using an EOS 750D camera (Canon). The particles in each well were counted and the data were presented as the mean ± SEM., calculated from five repeated experiments.

DiD-labeled cell adhesion assay

Cells were cultured to form a confluent monolayer in six-well plates, and 5 × 10^5 cells were labeled with 5 µM DiD (Invitrogen) in serum-free media for 30 min before being seeded onto the equivalent confluent cells. 2 h after coculture, media containing floating cells were discarded and adherent cells were trypsinized. The proportion of DiD-labeled adherent cells to the unlabeled cells was analyzed at 644 nM with flow cytometry.

Animal experiment

All experiments were performed under the approval of the Institutional Animal Care and Use Committee of the Shanghai Institute of Nutrition and Health, CAS (IACUC, SINH, CAS). All of the BALB/c nude mice in each experimental group were obtained from Shanghai SLAC Laboratory Animal Co., Ltd. For the lung metastasis model, 5 × 10^5 MC38 cells suspended in 100 µl serum-free DMEM were injected into the tail vein of 5-wk-old male nude mouse. 15/20 days after cell injection, the mice were sacrificed. The lungs were harvested and fixed in formalin for paraffin embedding.

To image tumors in live animals, 100 µl D-luciferin (final concentration: 15 mg/ml) was injected intraperitoneally into each mouse. After 15 min, mice were anesthetized by isoflurane and photographed in an IVIS imaging system (Xenogen).

Sequence analysis

Primary peptide sequence alignment was performed using Clustal Omega (available at http://www.ebi.ac.uk/Tools/msa/clustalo/). Secondary structure of XAF1 1–79 residues was calculated using Phyre2 (available at http://www.sbg.bio.ic.ac.uk/phyre2).

Statistical analyses

All data were analyzed using GraphPad Prism 9.0 (Macintosh). The results were represented as the means ± SEM. Shapiro-Wilk test was used to test the normality of data distribution, and Levene's test was used to test the differences between group variances. Statistical differences between two experimental groups with normally distributed data were analyzed by two-tailed unpaired Student's *t* test, data without normal distribution

were analyzed by Mann-Whitney test, and analysis between multiple groups was performed using one-way ANOVA with Bonferroni post hoc multiple comparison test. Correlations were analyzed by Pearson correlation analysis. All experiments were repeated three times or more independently. P value <0.05 was considered significant. Statistical analysis used in each panel was described in the figure legends.

Online supplemental material

Fig. S1 demonstrates that the mRNA expression of XAF1 is elevated in CRC tissues compared to normal tissues. Fig. S2 shows the effects of XAF1 on CRC cell growth and XAF1 regulates the expression of metastasis-related genes. Fig. S3 contains data disclosing the interactions between XAF1, RNF114, and VCP. Fig. S4 shows the identification of the deubiquitinating enzyme of RNF114 and the involvement of RNF114 in CRC cell migration. Fig. S5 reveals that XAF1 modulates cell–cell adhesion via regulating JUP protein stability. Table S1 shows the mass spectrometry results of XAF1-interacting proteins. Table S2 shows the mass spectrometry results of RNF114-interacting proteins. Table S3 demonstrates the correlation between XAF1 expression and the clinicopathologic features of CRC patients. Table S4 lists the primers for plasmid construction. Primers for shRNAs are listed in Table S5. Table S6 lists the primers for RT-qPCR analysis. Table S7 lists the antibodies used in this study.

Data availability

RNA-seq data supporting the results of this study are publicly available in the NCBI Sequence Read Archive database under BioProject ID PRJNA917429 (https://www.ncbi.nlm.nih.gov/bioproject/PRJNA917429). The mass spectrometry proteomics data have been deposited to the ProteomeXchange Consortium via the iProX partner repository with the dataset identifiers PXD041021 and PXD044440. Publicly available data generated by others were used by the authors, and the data analyzed in this study were obtained from the ProteomeXchange Consortium (PXD003936) and Gene Expression Omnibus with accession no. GSE131418. All the other data supporting the findings of this study are available within the article and its supplementary information. All additional information will be provided upon reasonable request to the authors.

Acknowledgments

We thank Zhong-Hui Weng, Yi-Fan Bu, and Lin Qiu from the Institutional Center for Shared Technologies and Facilities of SINH, CAS for technical assistance. We appreciate the New World Group for their charitable foundation to establish the Institute for Nutritional Sciences, SIBS, CAS-New World Joint Laboratory, which has given full support to this study.

This work was supported by the National Natural Science Foundation of China (81972757 and 82172950), Youth Innovation Promotion Association of Chinese Academy of Sciences grant (2017324) and Sanofi-SIBS 2018 Young Faculty Award to J.-J. Li, the Natural Science Foundation of Shanghai (23ZR1482300) to L. Long, and the National Natural Science Foundation of China (82030084 and 81730083) to D. Xie.

Author contributions: J. Xia, J.-J. Li, and L. Long conceived the project and designed the research studies. J. Xia performed most of the experiments described. N. Ma, Q. Shi, Q.-C. Liu, W. Zhang, Y.-K. Wang, H.-J. Cao, Y. Chen, and Q.-W. Zheng provided technical assistance in the mouse experiments, Q.-Z. Ni, S. Xu, B. Zhu, X.-S. Qiu, K. Ding, J.-Y. Huang, X. Liang, Y.-J. Xiang, X.-R. Zhang, L. Qiu, and W. Chen assisted with the in vitro assays. X. Wang provided clinical samples. D. Xie provided constructive advice. J. Xia analyzed data. J. Xia, J.-J. Li, and L. Long wrote the manuscript.

Disclosures: The authors declare no competing interests exist.

Submitted: 3 March 2023
Revised: 31 August 2023
Accepted: 16 October 2023

References

Aktary, Z., M. Alaee, and M. Pasdar. 2017. Beyond cell-cell adhesion: Plakoglobin and the regulation of tumorigenesis and metastasis. *Oncotarget*. 8:32270–32291. https://doi.org/10.18632/oncotarget.15650

Arrojo E Drigo, R., P. Egri, S. Jo, B. Gereben, and A.C. Bianco. 2013. The type II deiodinase is retrotranslocated to the cytoplasm and proteasomes via p97/Atx3 complex. *Mol. Endocrinol.* 27:2105–2115. https://doi.org/10.1210/me.2013-1281

Bailey, C.K., M.K. Mittal, S. Misra, and G. Chaudhuri. 2012. High motility of triple-negative breast cancer cells is due to repression of plakoglobin gene by metastasis modulator protein SLUG. *J. Biol. Chem.* 287:19472–19486. https://doi.org/10.1074/jbc.M112.345728

Biller, L.H., and D. Schrag. 2021. Diagnosis and treatment of metastatic colorectal cancer: A review. *JAMA*. 325:669–685. https://doi.org/10.1001/jama.2021.0106

Chen, K., J. Zeng, Y. Sun, W. Ouyang, G. Yu, H. Zhou, Y. Zhang, W. Yao, W. Xiao, J. Hu, et al. 2021. Junction plakoglobin regulates and destabilizes HIF2α to inhibit tumorigenesis of renal cell carcinoma. *Cancer Commun.* 41:316–332. https://doi.org/10.1002/cac2.12142

Chen, R.X., X. Chen, L.P. Xia, J.X. Zhang, Z.Z. Pan, X.D. Ma, K. Han, J.W. Chen, J.G. Judde, O. Deas, et al. 2019. N^6-methyladenosine modification of circNSUN2 facilitates cytoplasmic export and stabilizes HMGA2 to promote colorectal liver metastasis. *Nat. Commun.* 10:4695. https://doi.org/10.1038/s41467-019-12651-2

Chen, Y., L. Yang, Y. Qin, S. Liu, Y. Qiao, X. Wan, H. Zeng, X. Tang, M. Liu, and Y. Hou. 2020. Effects of differential distributed-JUP on the malignancy of gastric cancer. *J. Adv. Res.* 28:195–208. https://doi.org/10.1016/j.jare.2020.06.026

Choo, Z., R.Y. Koh, K. Wallis, T.J. Koh, C.H. Kuick, V. Sobrado, R.S. Kenchappa, A.H. Loh, S.Y. Soh, S. Schlisio, et al. 2016. XAF1 promotes neuroblastoma tumor suppression and is required for KIF1Bβ-mediated apoptosis. *Oncotarget*. 7:34229–34239. https://doi.org/10.18632/oncotarget.8748

Chung, S.K., M.G. Lee, B.K. Ryu, J.H. Lee, J. Han, D.S. Byun, K.S. Chae, K.Y. Lee, J.Y. Jang, H.J. Kim, and S.G. Chi. 2007. Frequent alteration of XAF1 in human colorectal cancers: Implication for tumor cell resistance to apoptotic stresses. *Gastroenterology*. 132:2459–2477. https://doi.org/10.1053/j.gastro.2007.04.024

Costantini, S., F. Capone, A. Polo, P. Bagnara, and A. Budillon. 2021. Valosin-containing protein (VCP)/p97: A prognostic biomarker and therapeutic target in cancer. *Int. J. Mol. Sci.* 22:10177. https://doi.org/10.3390/ijms221810177

Ernst, R., B. Mueller, H.L. Ploegh, and C. Schlieker. 2009. The otubain YOD1 is a deubiquitinating enzyme that associates with p97 to facilitate protein dislocation from the ER. *Mol. Cell.* 36:28–38. https://doi.org/10.1016/j.molcel.2009.09.016

Feng, Z., L. Li, Q. Zeng, Y. Zhang, Y. Tu, W. Chen, X. Shu, A. Wu, J. Xiong, Y. Cao, and Z. Li. 2022. RNF114 silencing inhibits the proliferation and metastasis of gastric cancer. *J. Cancer*. 13:565–578. https://doi.org/10.7150/jca.62033

Fu, Q., Y. Jiang, D. Zhang, X. Liu, J. Guo, and J. Zhao. 2016. Valosin-containing protein (VCP) promotes the growth, invasion, and metastasis of

colorectal cancer through activation of STAT3 signaling. *Mol. Cell. Biochem.* 418:189–198. https://doi.org/10.1007/s11010-016-2746-

Gwon, Y., B.A. Maxwell, R.M. Kolaitis, P. Zhang, H.J. Kim, and J.P. Taylor. 2021. Ubiquitination of G3BP1 mediates stress granule disassembly in a context-specific manner. *Science.* 372:eabf6548. https://doi.org/10.1126/science.abf6548

Han, J., Y.L. Kim, K.W. Lee, N.G. Her, T.K. Ha, S. Yoon, S.I. Jeong, J.H. Lee, M.J. Kang, M.G. Lee, et al. 2013. ZNF313 is a novel cell cycle activator with an E3 ligase activity inhibiting cellular senescence by destabilizing p21(WAF1.). *Cell Death Differ.* 20:1055–1067. https://doi.org/10.1038/cdd.2013.33

Han, W., Q. Chen, J. Cui, Y. Zhao, M. Li, and X. Li. 2022. E3 ubiquitin ligase RNF114 promotes vesicular stomatitis virus replication via inhibiting type I interferon production. *Microb. Pathog.* 167:105569. https://doi.org/10.1016/j.micpath.2022.105569

Hao, X., F. Han, B. Ma, N. Zhang, H. Chen, X. Jiang, L. Yin, W. Liu, L. Ao, J. Cao, and J. Liu. 2018. SOX30 is a key regulator of desmosomal gene suppressing tumor growth and metastasis in lung adenocarcinoma. *J. Exp. Clin. Cancer Res.* 37:111. https://doi.org/10.1186/s13046-018-0778-3

Heidelberger, J.B., A. Voigt, M.E. Borisova, G. Petrosino, S. Ruf, S.A. Wagner, and P. Beli. 2018. Proteomic profiling of VCP substrates links VCP to K6-linked ubiquitylation and c-Myc function. *EMBO Rep.* 19:e44754. https://doi.org/10.15252/embr.201744754

Hill, S.M., L. Wrobel, A. Ashkenazi, M. Fernandez-Estevez, K. Tan, R.W. Bürli, and D.C. Rubinsztein. 2021. VCP/p97 regulates Beclin-1-dependent autophagy initiation. *Nat. Chem. Biol.* 17:448–455. https://doi.org/10.1038/s41589-020-00726-x

Holcik, M., and R.G. Korneluk. 2001. XIAP, the guardian angel. *Nat. Rev. Mol. Cell Biol.* 2:550–556. https://doi.org/10.1038/35080103

Jeong, S.I., J.W. Kim, K.P. Ko, B.K. Ryu, M.G. Lee, H.J. Kim, and S.G. Chi. 2018. XAF1 forms a positive feedback loop with IRF-1 to drive apoptotic stress response and suppress tumorigenesis. *Cell Death Dis.* 9:806. https://doi.org/10.1038/s41419-018-0867-4

Kamal, Y., S.L. Schmit, H.J. Hoehn, C.I. Amos, and H.R. Frost. 2019. Transcriptomic differences between primary colorectal adenocarcinomas and distant metastases reveal metastatic colorectal cancer subtypes. *Cancer Res.* 79:4227–4241. https://doi.org/10.1158/0008-5472.CAN-18-3945

Lee, K.W., H.R. Hong, J.S. Lim, K.P. Ko, M.G. Lee, and S.G. Chi. 2022. XAF1 drives apoptotic switch of endoplasmic reticulum stress response through destabilization of GRP78 and CHIP. *Cell Death Dis.* 13:655. https://doi.org/10.1038/s41419-022-05112-0

Lee, M.G., J. Han, S.I. Jeong, N.G. Her, J.H. Lee, T.K. Ha, M.J. Kang, B.K. Ryu, and S.G. Chi. 2014. XAF1 directs apoptotic switch of p53 signaling through activation of HIPK2 and ZNF313. *Proc. Natl. Acad. Sci. USA.* 111:15532–15537. https://doi.org/10.1073/pnas.1411746111

Li, J., D. Swope, N. Raess, L. Cheng, E.J. Muller, and G.L. Radice. 2011. Cardiac tissue-restricted deletion of plakoglobin results in progressive cardiomyopathy and activation of {beta}-catenin signaling. *Mol. Cell. Biol.* 31:1134–1144. https://doi.org/10.1128/MCB.01025-10

Li, Y., K. Hu, X. Xiao, W. Wu, H. Yan, H. Chen, Z. Chen, and D. Yin. 2018. FBW7 suppresses cell proliferation and G2/M cell cycle transition via promoting γ-catenin K63-linked ubiquitylation. *Biochem. Biophys. Res. Commun.* 497:473–479. https://doi.org/10.1016/j.bbrc.2018.01.192

Lim, J.S., K.W. Lee, K.P. Ko, S.I. Jeong, B.K. Ryu, M.G. Lee, and S.G. Chi. 2022. XAF1 destabilizes estrogen receptor α through the assembly of a BRCA1-mediated destruction complex and promotes estrogen-induced apoptosis. *Oncogene.* 41:2897–2908. https://doi.org/10.1038/s41388-022-02315-9

Liston, P., W.G. Fong, N.L. Kelly, S. Toji, T. Miyazaki, D. Conte, K. Tamai, C.G. Craig, M.W. McBurney, and R.G. Korneluk. 2001. Identification of XAF1 as an antagonist of XIAP anti-Caspase activity. *Nat. Cell Biol.* 3:128–133. https://doi.org/10.1038/35055027

Liu, B.Q., R.B. Liu, W.P. Li, X.T. Mao, Y.N. Li, T. Huang, H.L. Wang, H.T. Chen, J.Y. Zhong, B. Yang, et al. 2023. XAF1 prevents hyperproduction of type I interferon upon viral infection by targeting IRF7. *EMBO Rep.* 24:e55387. https://doi.org/10.15252/embr.202255387

Magnaghi, P., R. D'Alessio, B. Valsasina, N. Avanzi, S. Rizzi, D. Asa, F. Gasparri, L. Cozzi, U. Cucchi, C. Orrenius, et al. 2013. Covalent and allosteric inhibitors of the ATPase VCP/p97 induce cancer cell death. *Nat. Chem. Biol.* 9:548–556. https://doi.org/10.1038/nchembio.1313

Malki, A., R.A. ElRuz, I. Gupta, A. Allouch, S. Vranic, and A.E. Al Moustafa. 2020. Molecular mechanisms of colon cancer progression and metastasis: Recent insights and advancements. *Int. J. Mol. Sci.* 22:130. https://doi.org/10.3390/ijms22010130

Meyer, H., M. Bug, and S. Bremer. 2012. Emerging functions of the VCP/p97 AAA-ATPase in the ubiquitin system. *Nat. Cell Biol.* 14:117–123. https://doi.org/10.1038/ncb2407

Pan, M., Y. Yu, H. Ai, Q. Zheng, Y. Xie, L. Liu, and M. Zhao. 2021. Mechanistic insight into substrate processing and allosteric inhibition of human p97. *Nat. Struct. Mol. Biol.* 28:614–625. https://doi.org/10.1038/s41594-021-00617-2

Pu, Z., D.G. Duda, Y. Zhu, S. Pei, X. Wang, Y. Huang, P. Yi, Z. Huang, F. Peng, X. Hu, and X. Fan. 2022. VCP interaction with HMGB1 promotes hepatocellular carcinoma progression by activating the PI3K/AKT/mTOR pathway. *J. Transl. Med.* 20:212. https://doi.org/10.1186/s12967-022-03416-5

Siegel, R.L., N.S. Wagle, A. Cercek, R.A. Smith, and A. Jemal. 2023. Colorectal cancer statistics, 2023. *CA Cancer J. Clin.* 73:233–254. https://doi.org/10.3322/caac.21772

Sung, H., J. Ferlay, R.L. Siegel, M. Laversanne, I. Soerjomataram, A. Jemal, and F. Bray. 2021. Global cancer statistics 2020: GLOBOCAN estimates of incidence and mortality worldwide for 36 cancers in 185 countries. *CA Cancer J. Clin.* 71:209–249. https://doi.org/10.3322/caac.21660

Tang, W.K., D. Li, C.C. Li, L. Esser, R. Dai, L. Guo, and D. Xia. 2010. A novel ATP-dependent conformation in p97 N-D1 fragment revealed by crystal structures of disease-related mutants. *EMBO J.* 29:2217–2229. https://doi.org/10.1038/emboj.2010.104

Tse, M.K., C.K. Cho, W.F. Wong, B. Zou, S.K. Hui, B.C. Wong, and K.H. Sze. 2012. Domain organization of XAF1 and the identification and characterization of XIAP(RING) -binding domain of XAF1. *Protein Sci.* 21:1418–1428. https://doi.org/10.1002/pro.2126

Turakhiya, A., S.R. Meyer, G. Marincola, S. Böhm, J.T. Vanselow, A. Schlosser, K. Hofmann, and A. Buchberger. 2018. ZFAND1 recruits p97 and the 26S proteasome to promote the clearance of arsenite-induced stress granules. *Mol. Cell.* 70:906–919.e7. https://doi.org/10.1016/j.molcel.2018.04.021

van den Boom, J., and H. Meyer. 2018. VCP/p97-Mediated unfolding as a principle in protein homeostasis and signaling. *Mol. Cell.* 69:182–194. https://doi.org/10.1016/j.molcel.2017.10.028

van Wijk, S.J., S. Fulda, I. Dikic, and M. Heilemann. 2019. Visualizing ubiquitination in mammalian cells. *EMBO Rep.* 20:e46520. https://doi.org/10.15252/embr.201846520

Wang, Y., H. Mao, Q. Hao, Y. Wang, Y. Yang, L. Shen, S. Huang, and P. Liu. 2012. Association of expression of XIAP-associated factor 1 (XAF1) with clinicopathologic factors, overall survival, microvessel density and cisplatin-resistance in ovarian cancer. *Regul. Pept.* 178:36–42. https://doi.org/10.1016/j.regpep.2012.06.005

Wang, Y., J. Zhang, Y.J. Li, N.N. Yu, W.T. Liu, J.Z. Liang, W.W. Xu, Z.H. Sun, B. Li, and Q.Y. He. 2021. MEST promotes lung cancer invasion and metastasis by interacting with VCP to activate NF-κB signaling. *J. Exp. Clin. Cancer Res.* 40:301. https://doi.org/10.1186/s13046-021-02107-1

Weihl, C.C., S. Dalal, A. Pestronk, and P.I. Hanson. 2006. Inclusion body myopathy-associated mutations in p97/VCP impair endoplasmic reticulum-associated degradation. *Hum. Mol. Genet.* 15:189–199. https://doi.org/10.1093/hmg/ddi426

Yang, Y., C. Zhou, Y. Wang, W. Liu, C. Liu, L. Wang, Y. Liu, Y. Shang, M. Li, S. Zhou, et al. 2017. The E3 ubiquitin ligase RNF114 and TAB1 degradation are required for maternal-to-zygotic transition. *EMBO Rep.* 18:205–216. https://doi.org/10.15252/embr.201642573

Yeung, H.O., P. Kloppsteck, H. Niwa, R.L. Isaacson, S. Matthews, X. Zhang, and P.S. Freemont. 2008. Insights into adaptor binding to the AAA protein p97. *Biochem. Soc. Trans.* 36:62–67. https://doi.org/10.1042/BST0360062

Zhang, X., and Y. Wang. 2015. Cell cycle regulation of VCIP135 deubiquitinase activity and function in p97/p47-mediated Golgi reassembly. *Mol. Biol. Cell.* 26:2242–2251. https://doi.org/10.1091/mbc.E15-01-0041

Zhao, Y., X. Liang, L. Wei, Y. Liu, J. Liu, H. Feng, F. Zheng, Y. Wang, H. Ma, and J. Wu. 2021. RNF114 suppresses metastasis through regulation of PARP10 in cervical cancer cells. *Cancer Commun.* 41:187–191. https://doi.org/10.1002/cac2.12132

Zhou, S., Y. Guo, H. Sun, L. Liu, L. Yao, C. Liu, Y. He, S. Cao, C. Zhou, M. Li, et al. 2021. Maternal RNF114-mediated target substrate degradation regulates zygotic genome activation in mouse embryos. *Development.* 148:dev199426. https://doi.org/10.1242/dev.199426

Zhu, G., L. Pei, H. Xia, Q. Tang, and F. Bi. 2021. Role of oncogenic KRAS in the prognosis, diagnosis and treatment of colorectal cancer. *Mol. Cancer.* 20:143. https://doi.org/10.1186/s12943-021-01441-4

Supplemental material

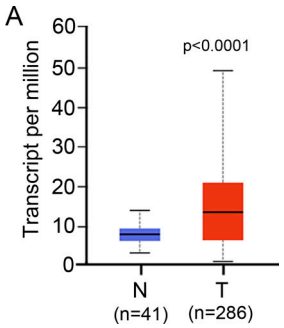

Figure S1. **The expression XAF1 is elevated in CRC tissues. (A)** The mRNA expression of XAF1 in normal (N) and CRC tumor (T) tissues was analyzed using the UALCAN database.

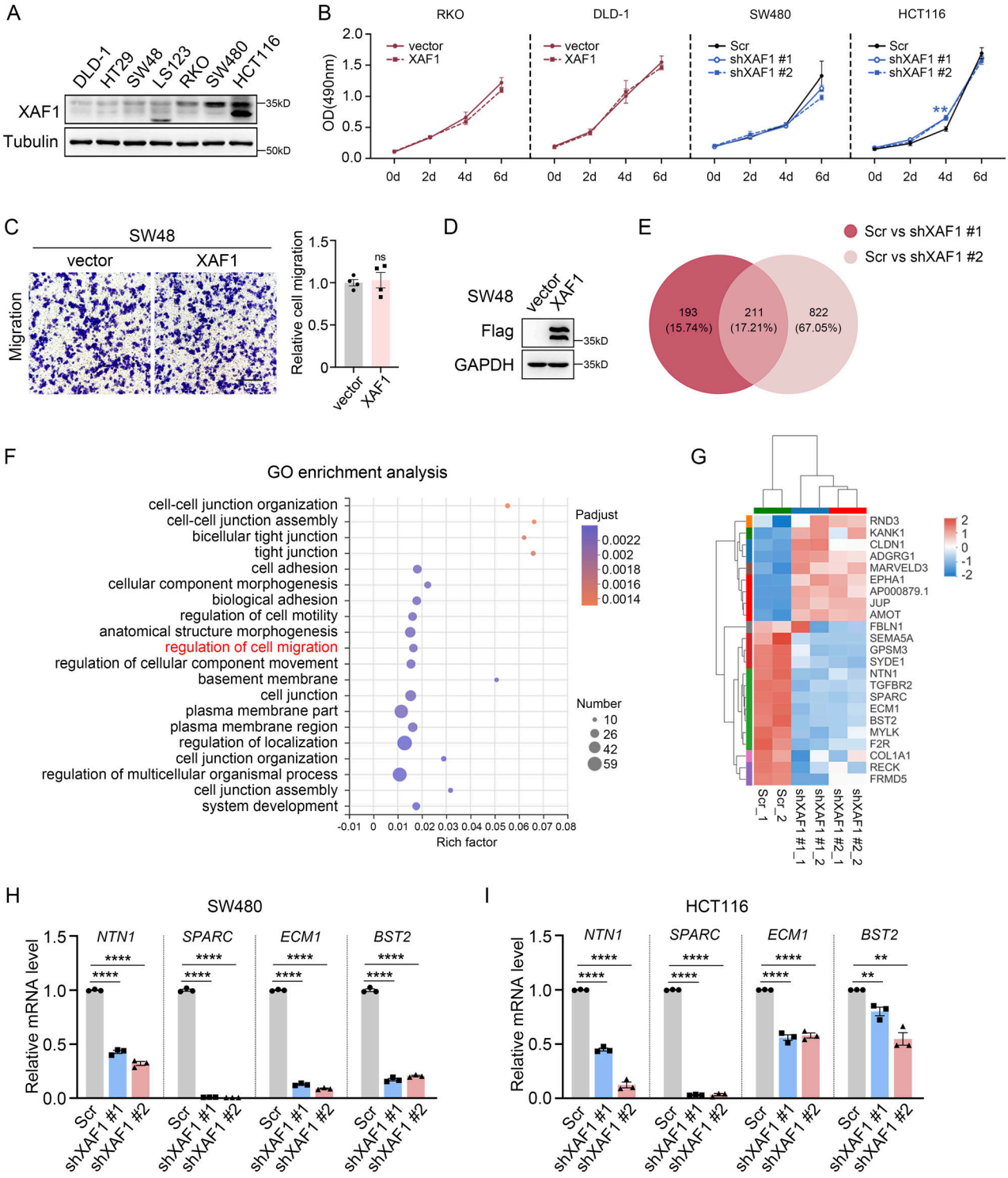

Figure S2. **XAF1 affects CRC cell metastasis. (A)** The protein level of XAF1 in seven CRC cell lines was examined by Western blot. **(B)** MTT assay examining the effects of XAF1 on the growth of RKO, DLD-1, SW480, and HCT116 cells, *n* = 3 replicates. Scr, Scramble. **(C)** Migration capabilities of control and XAF1-overexpressing SW48 cells were examined by transwell assay. Left: Representative images. Scale bar, 100 µm. Right: Histograms representing the number of migrated cells relative to control, *n* = 4 random fields. **(D)** Western blot analysis of the overexpression efficiency of XAF1 in SW48 cells. **(E)** Venn diagram of differentially expressed genes (DEGs). Scr, Scramble. **(F)** The top 20 enriched GO terms of 211 DEGs based on the RNA seq analysis of control and XAF1 knockdown SW480 cells. **(G)** Heat map showing differential gene expression between control and XAF1 knockdown cells in the item "regulation of cell migration" in F. Scr, Scramble. **(H and I)** The expression of migration-promoting genes was validated by qPCR in control and XAF1 knockdown SW480 (H) and HCT116 (I) cells, *n* = 3 replicates. Scr, Scramble. The data in B were analyzed with one-way ANOVA with Bonferroni post-hoc multiple comparison test. The data in C, H, and I were analyzed by two-tailed unpaired Student's *t* test. All results were represented as the mean ± SEM. ns: not significant, **P < 0.01, ****P <0.0001. Source data are available for this figure: SourceData FS2.

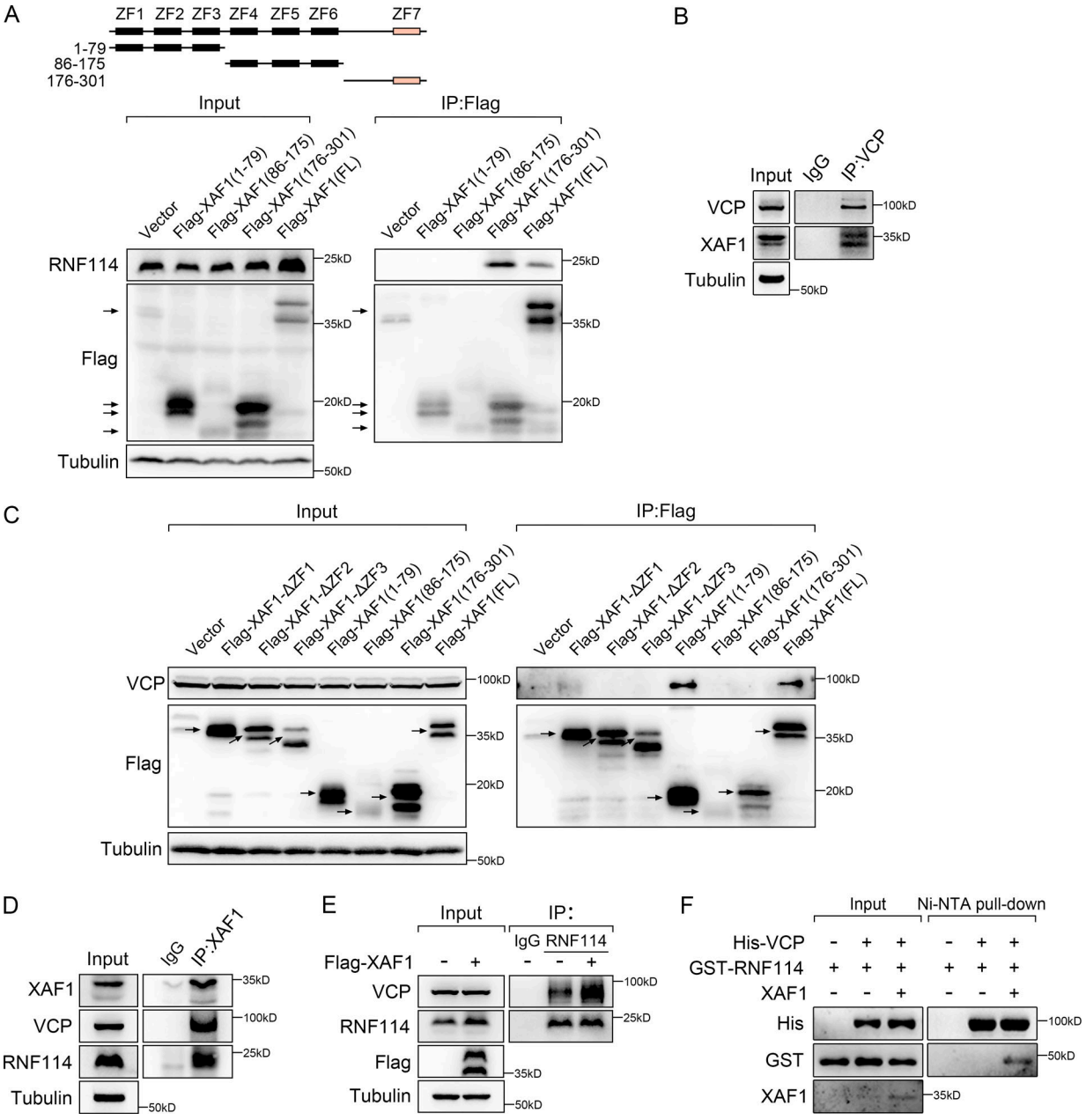

Figure S3. **Interactions between XAF1, RNF114, and VCP. (A)** The interactions between endogenous RNF114 and truncated XAF1 mutants were examined by co-IP assay in 293T cells. **(B)** The interaction between endogenous VCP and XAF1 was assessed by co-IP. IgG was used as a negative control. **(C)** The interactions between endogenous VCP and truncated XAF1 mutants were examined by co-IP assay in 293T cells. **(D)** The interactions between endogenous XAF1, RNF114, and VCP were examined by co-IP. IgG was used as a negative control. **(E)** The interaction between VCP and RNF114 in control and XAF1-overexpressing cells was examined by co-IP. IgG was used as a negative control. **(F)** Ni-NTA pull-down assay was used to detect the interaction between VCP and RNF114 in the presence or absence of XAF1 in vitro. Source data are available for this figure: SourceData FS3.

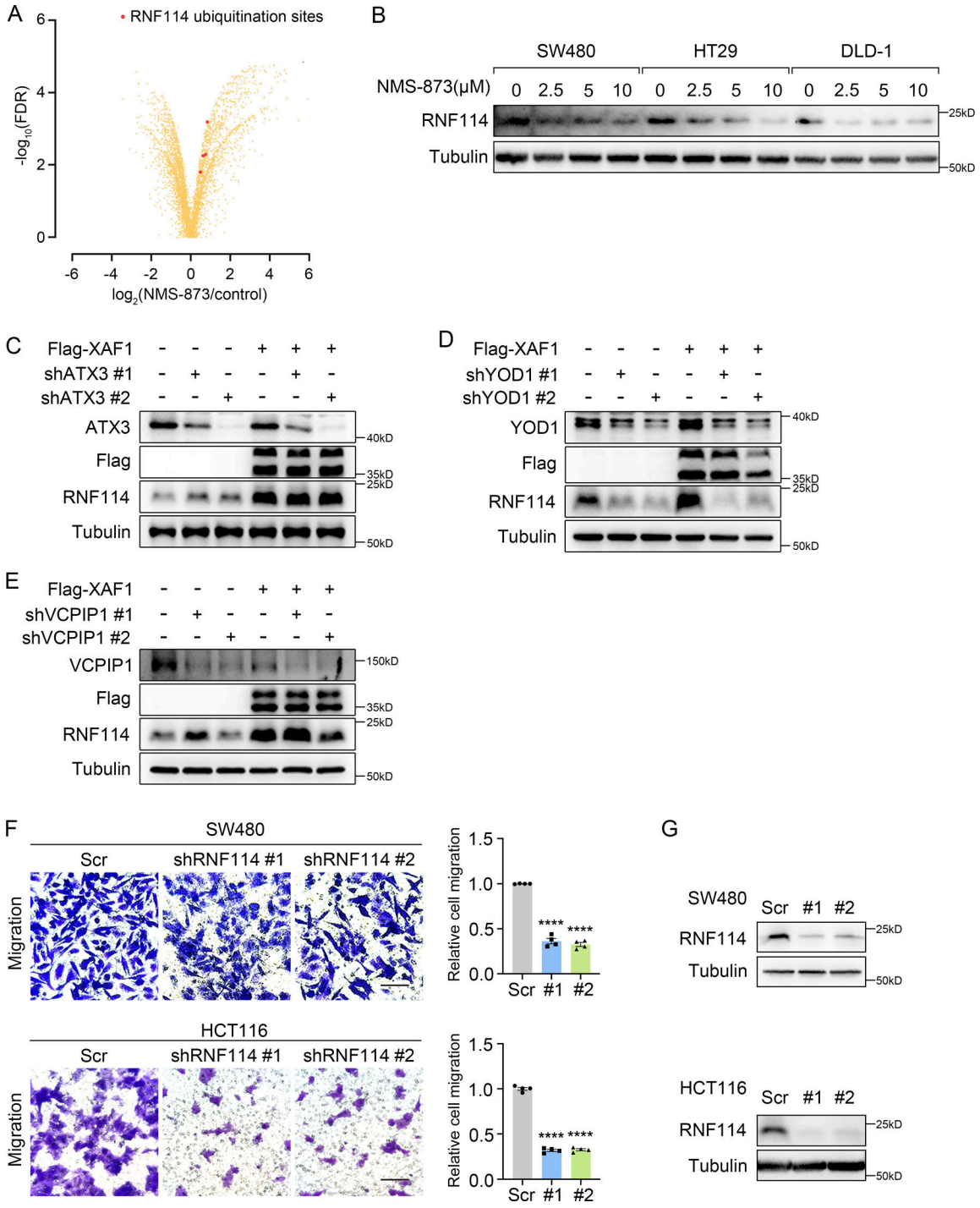

Figure S4. **Regulation of RNF114 and its involvement in CRC cell migration. (A)** Identification of significantly altered ubiquitylation sites after NMS-873 treatment. Red dots indicated the ubiquitination sites on RNF114. **(B)** The influence of NMS-873 on RNF114 was examined in CRC cells. Cells were treated with NMS-873 for 8 h. **(C–E)** The influence of ATX3 (C), YOD1 (D), and VCPIP1 (E) knockdown on RNF114 was examined in control and XAF1-overexpressing DLD-1 cells. **(F)** Migration abilities of control and RNF114 knockdown CRC cells were assessed by transwell assay. Left: Representative images. Scale bar, 100 μm. Right: Histograms representing the number of migrated cells relative to control, *n* = 4 random fields. Scr, Scramble. **(G)** Western blot examining RNF114 knockdown efficiency in CRC cells. Scr, Scramble. The data in F were analyzed by two-tailed unpaired Student's *t* test and represented as the mean ± SEM. ****P < 0.0001. Source data are available for this figure: SourceData FS4.

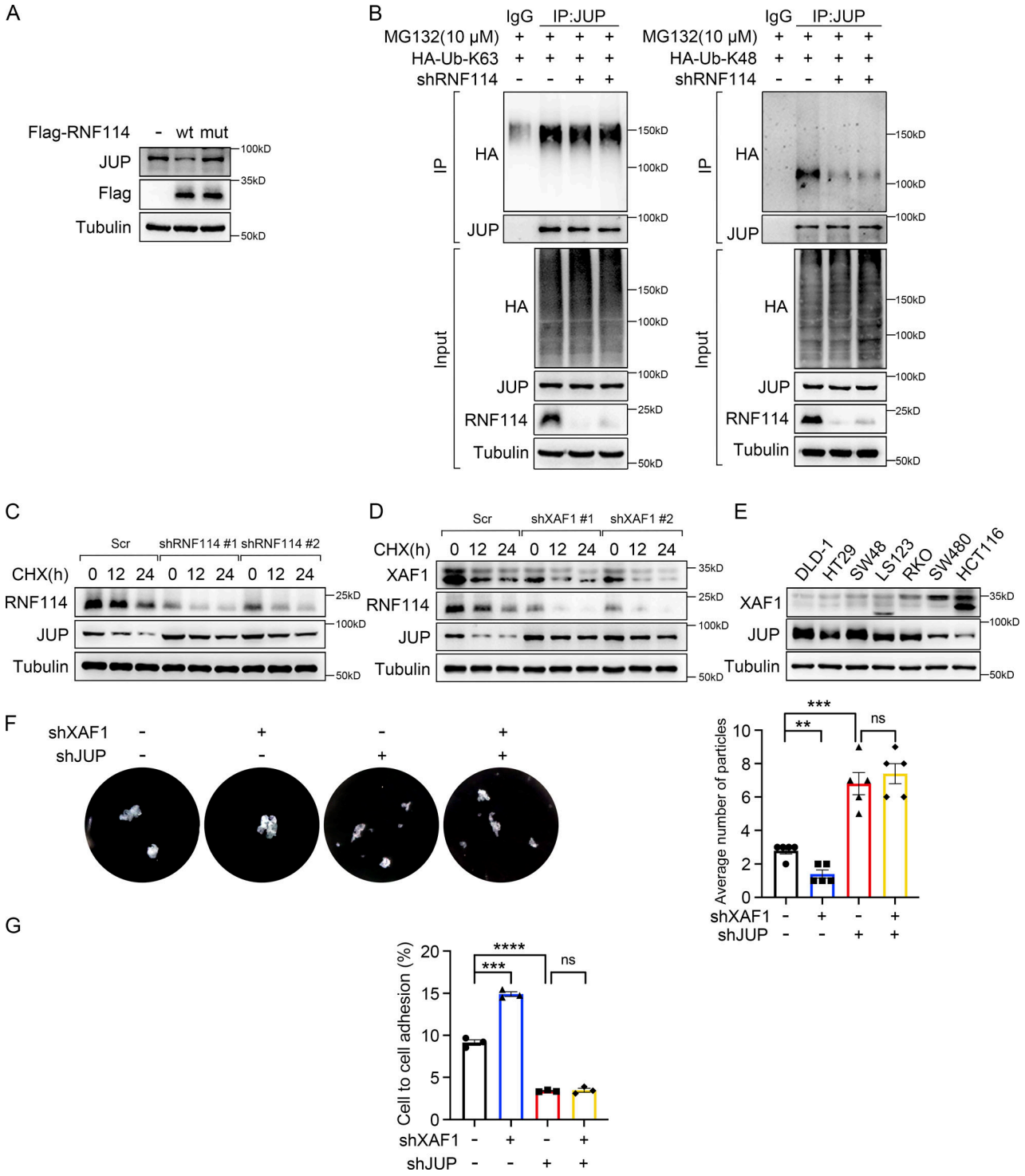

Figure S5. **XAF1 modulates cell–cell adhesion by regulating protein stability of JUP. (A)** The expression of JUP was examined in 293T cells transfected with vector, wild-type, and mutant RNF114, respectively. **(B)** The type of ubiquitin chains on JUP was examined using the constructs expressing HA-Ub (K63 only) and HA-Ub (K48 only) ubiquitin mutants. Cells were treated with 10 μM MG132 for 8 h. IgG was used as a negative control. **(C)** Cycloheximide chase assay was performed in control and RNF114-deficient HCT116 cells to examine the protein stability of JUP. Cells were treated with 50 μg/ml CHX. Scr, Scramble. **(D)** Cycloheximide chase assay was performed in control and XAF1-deficient HCT116 cells to examine the protein stability of RNF114 and JUP. Cells were treated with 50 μg/ml CHX. Scr, Scramble. **(E)** The protein level of XAF1 and JUP in seven CRC cell lines was examined by Western blot. This result and Fig. S2 A were from the same experiment. **(F)** Dispase-based dissociation assay examining the cell–cell adhesion in control, XAF1 knockdown, JUP knockdown, and XAF1/JUP double knockdown SW480 cells. Left: Representative images. Right: Histograms of the average number of particles, $n = 5$ replicates. **(G)** The proportion of cells adhering to the confluent monolayer was assessed using DiD Cell-Labeling reagent, $n = 3$ replicates. The data in F and G were analyzed with one-way ANOVA with Bonferroni post-hoc multiple comparison test and represented as the mean ± SEM. ns: not significant, **P < 0.01, ***P < 0.001, ****P < 0.0001. Source data are available for this figure: SourceData FS5.

Provided online are seven tables. Table S1 shows the mass spectrometry results of XAF1-interacting proteins. Table S2 shows the mass spectrometry results of RNF114-interacting proteins. Table S3 shows the correlation between XAF1 expression and clinicopathologic features of CRC patients. Table S4 shows primers for gene cloning. Table S5 shows primers for shRNAs. Table S6 shows primers for RT-qPCR. Table S7 lists the antibodies used in this study.